

Seasonal Assessment Of Cross-Shore Morphodynamic Behaviour Of Wave-Dominated Beaches Using Data-Driven Analysis

Lynda-Uta Edet Okon^{1,2,4 *}, Jaya Kumar Seelam^{1,3}

LEO: ORCID® 0000-0002-7252-4220

JKS: ORCID® 0000-0003-0406-3204

¹ Ocean Engineering Division, CSIR-National Institute of Oceanography, Goa, India

² Bharathidasan University, Tiruchirappalli, India

³ Academy of Scientific and Innovative Research, School of Oceanography, Goa, India

⁴ Physical Oceanography Unit, Institute of Oceanography, University of Calabar, Nigeria

* Corresponding author email: lyndaokon@gmail.com

Abstract

Four years of data-driven analyses - Empirical Orthogonal Function (EOF) analysis and Canonical Correlation Analysis (CCA), were performed for North and South Goa beach profile datasets (2018-2021) to improve data processing and interpretation. The goal is to understand the significant cross-shore morphodynamic variations by evaluating dominating EOF patterns and discovering inherent correlations between beach-face slope, nearshore parameters, and environmentally sensitive sediment grain size parameters using CCA. The method separates the data's spatial and temporal dependencies, allowing beach-face changes to be characterised as a linear combination of space and time functions. After analysing data sets from 45 surveys conducted during the southwest, northeast, and pre-monsoon seasons, three statistically significant EOF modes were identified. The outcomes of the seasonally sampled data differed, with most variations in the beach-face configuration explained by the first three eigenfunctions, corresponding to the three largest eigenvalues. The largest eigenfunction reflects the average slope of the beach face. The slope of the second eigenfunction varies the most from the mean. The coastline is generally in an intermediate stage, with episodic beach morphology variation. The EOF investigation confirms the widely known hypothesis that the beach face is the most morphodynamically active zone, with North and South Goa beaches displaying year-round rhythmic variation, with the slope modulation most evident in the northeast monsoon season. The multivariate CCA strongly links wave parameters and beach-face slope. Similarly, a strong correlation is observed between the beach-face slope and sediment grain size parameters, particularly the sediment gradation indices, D_{90}/D_{10} and D_{84}/D_{16} . The results indicate that the methods are reliable for analysing and interpreting beach-face variation behaviour and controlling physical processes and highlight the need for long-term spatio-temporal analysis and a guide for coastline management.

Keywords: Data-driven analysis, Cross-shore morphodynamics, Beach-face slope, seasonal climate, EOF, CCA, spatial and temporal analysis, cross-correlation.

Introduction

Beaches are among the most active dynamic sedimentary environments on the globe and are influenced by variables such as sea level rise, sediment supply, waves and tides, and anthropogenic modifications (Luijendijk et al. 2018; Tamura et al. 2018; Hein et al. 2019). They provide, among other benefits, a range of ecological functions, vital flood defence measures, and attractive tourist destinations (Martínez et al. 2008). Beach morphology sheds light on the factors that control seasonal sediment movement on beaches (Wright and Short, 1984). Over the past several decades, significant efforts have been made to enhance the ability to identify and quantify morphological changes at different spatial and temporal scales and to examine the connections between beach sediment particle size, beach face slope, and beach exposure in response to storm sequences (Miller and Dean 2007; Elias and Hansen 2013; Karunarathna and Reeve 2013). The interaction between nearshore processes (including waves, wind activity, tidal currents, infiltration, and exfiltration) and beach morphology generates an incredibly fascinating dynamic system. Field measurements, experimental surveys, and numerical models spanning various periods have also been employed to examine the links between beach change and its controlling processes (Larson et al. 2000; Karunarathna et al. 2012a, 2016; Medellín et al. 2018; Medellín and Torres-Freyermuth 2019; Chowdhury et al. 2020). According to Larson and Kraus (1995) this process includes various components at different time and space scales, making it a challenging yet essential research focus. Understanding the fundamental morphological processes is also required to efficiently design coastal protection or development activities.

The beach face is the part of the beach that often interacts with wave run-up; the equilibrium of forces pushing sediment governs its shape. It refers to the space between the seaward berm and the mean low water level or the maximum wave uprush at high tide (Mangor et al. 2017). The temporal evolution of the beach face and sand quantities is essential for coastal planning and hazard evaluation since it has significant socioecological ramifications. Beach-face slope and sediment particle size are the two distinctive characteristics of beach morphology that scientists have studied for decades (Reis and Gama 2010; Bujan et al. 2019; McFall 2019; Cabezas-Rabadán et al. 2021; Woodruff et al. 2021; Cheng et al. 2022). Wave motion, which includes wave impact, uprush, and backwash, is the most important component determining the morphology of the beach face (Bascom 1951a; Reis and Gama 2010; Bergillos et al. 2017). Typically, an investigator's assessment of the highest run-up is utilised to estimate the beach face width operationally at any particular location. For beaches with simple slopes, this is typically defined as the distance between the single berms (Bujan et al. 2019). When there are many berms, the most common approach is to measure the beach up to the tallest

berm, with each berm having a different run-up elevation and return period (Muñoz-Perez and Medina 2010; McCall et al. 2015; Bujan et al. 2019). Cross-shore movements occur on a spectrum of timelines, endangering infrastructure, public safety, and the integrity of natural and artificial coastal barriers (Larson et al. 2003; Masselink et al. 2008; Lemos et al. 2018). Hence, beach-face slope research is necessary for comprehending and analysing wave run-up, total swash excursion at the beach, and potential inundation dangers along the Goa coast (Oliveira et al. 2017). In addition, it provides information for swimming safety and is a proxy for the hydrodynamics of the surf zone (Vos et al. 2020).

Similarly, the sediment particle size of the beach is an essential element as it affects how the beach responds to the previously indicated physical pushing forces (Wright and Short 1984; Buscombe and Masselink 2006). It is utilised to classify and specify beach states (Masselink et al. 2008). Bascom (1951) gave the first definitive evidence of the relationship between the beach face and wave climate. Depending on wave state and cross-shore topography, sand beaches portray varying degrees of sorting (Cabezas-Rabadán et al. 2021). Although materials are sorted more precisely down the coast, sediment sources and coastal obstacles (such as headlands and artificial structures) tend to bias and restrict the types and sizes of materials that arrive on sandy beaches (Hein et al. 2019).

It is crucial to comprehend how a beach reacts to large waves, and the ensuing calm intervals, particularly as sea levels continue to rise and climate change may affect the frequency and intensity of storms (Ludka et al. 2015). Given that incident wave climate, nearshore currents, sediment size and distribution, and sea level all influence cross-shore beach profile variability, it is preferable to measure and account for these variables through data-driven empirical investigation (Stive and de Vriend 1995; Karunarathna and Reeve 2013).

Data-driven Modeling is founded on the evaluation of field-based datasets using empirical approaches (Karunarathna et al. 2012b). Assuming that data collecting locations have an acceptable spatial and temporal resolution, field measurement datasets contain all information regarding the spatial and temporal patterns of physical processes occurring in the coastal zone. Data-driven models, despite their data-heavy nature, do not require coefficient calibration. Two data-driven empirical analyses used in coastal studies - Empirical orthogonal function analysis (EOF) and Canonical Correlation Analysis (CCA), employ sophisticated statistical "reduced physics models" to identify patterns of change over time and space in a set of indicators. They also account for many dominant processes responsible for altering coastal morphology. Theoretically, a simplified physics equation can characterise these processes and provide forecasts throughout the essential timescales for coastal management planning.

Empirical orthogonal function analysis (EOF) is employed in coastal studies to evaluate seasonal cross-shore variation as a function of spatial and temporal modes of variance (Dean and Dalrymple 2010). This approach generates a regression matrix to predict beach profiles based on expected wave conditions. Their predictive performance is site-specific and reliant on the spectrum of observed behaviour. The advantage of EOF is that it selects the smallest subset of functions (eigenfunctions) capable of highlighting spatial and temporal information, with the first eigenfunction accounting for most data variation. The first three eigenfunctions for the Winant et al. (1975) data sets were associated with physical modes of variability exhibiting the mean beach profile and seasonal shift between beach profile configurations (Miller and Dean 2007). Karunarathna et al. (2016) analysed regional and temporal patterns utilising eigenfunctions built from decades of data-based links between incident waves and cross-sectional profile variations created in several global locations and sediment compositions (medium to fine sand, sand to gravel). Using routinely recorded beach profiles, Jeevivek et al. (2018, 2019) and Miles et al. (2019) explored medium-term cross-shore profile behaviour, such as changes in coastline position, intertidal bar movement, and profile shape variability. In their trials, EOFs were utilised to demonstrate seasonal and interannual changes in wave climate and profile behaviour.

In contrast, Canonical Correlation Analysis (CCA) identifies any connections between the behaviour of two variables and gives a regression matrix that can be utilised to create predictions in coastal engineering research. This technique has been widely implemented in various fields, including coastal engineering (Larson et al. 2000), for analysing the beach's response to wave action and meteorology and climatology for weather forecasting. (Reeve et al. 2016) used it to forecast beach profiles using wave probability density functions. Regarding capturing correlations and variability among nearshore variables, CCA-based hindcasts have demonstrated a respectable level of performance (Karunarathna et al. 2015; Miller et al. 2015)

Although the accuracy of profile change prediction utilising processed-based and numerical models has increased, these techniques can be computationally expensive, and the complexity of the physics behind the models can lead to discrepancies between observed data and model outputs (Miller and Dean 2007; Lemke et al. 2014). Comparative studies of locations focussing on sediment heterogeneity are rare, in contrast to research on changes in cross-shore morphodynamics of distinct beach types under various wave and hydrodynamic situations. Due to the primary sediment particle size, two sites with distinct site characteristics may behave very differently under identical wave and hydrodynamic conditions. Nevertheless, hindcasts based on EOF and CCA analyses indicate that

these techniques can generate good outcomes in different time scales, assuming the accuracy of the wave forecast (Karunaratna et al. 2012b, 2015c, 2016; Chatzirodou et al. 2017).

This research investigates the advantages of incorporating wave parameters and grain size into data-driven EOFs and CCA models for beach expansion. This study is based on four years of beach surveys conducted on various beaches in Goa. Using these data-driven analytical methods, the primary objectives are to identify critical patterns of variability between nearshore parameters, beach face morphology, and morpho-sedimentary parameters along India's Central West Coast to determine the primary drivers of beach profile variation and evaluate the reliability of these empirical models for studies of hydro-morphodynamic interactions. Besides from these crucial reasons, this study is vital in light of current utilisation for artisanal and ecotourism purposes to provide information for beach swimming safety (Short 1993). Understanding the relationship between these physical components and beach change along the Goa coast is essential for evaluating the stability of these beaches in response to nearshore activity, as coastal scientists, engineers, and beach managers rely heavily on this information when making management and mitigation decisions.

The structure of the paper is as follows: The second section provides thorough information regarding the study site, data sets used, and analysis processes. In addition, it discusses EOF-based data analysis as a method for assessing the regional and temporal evolution of beach-face slopes and provides a pre-filtering component of the CCA method. The third section provides the essential findings of the investigation. In sections 4 and 5, the analysis and findings are discussed and concluded.

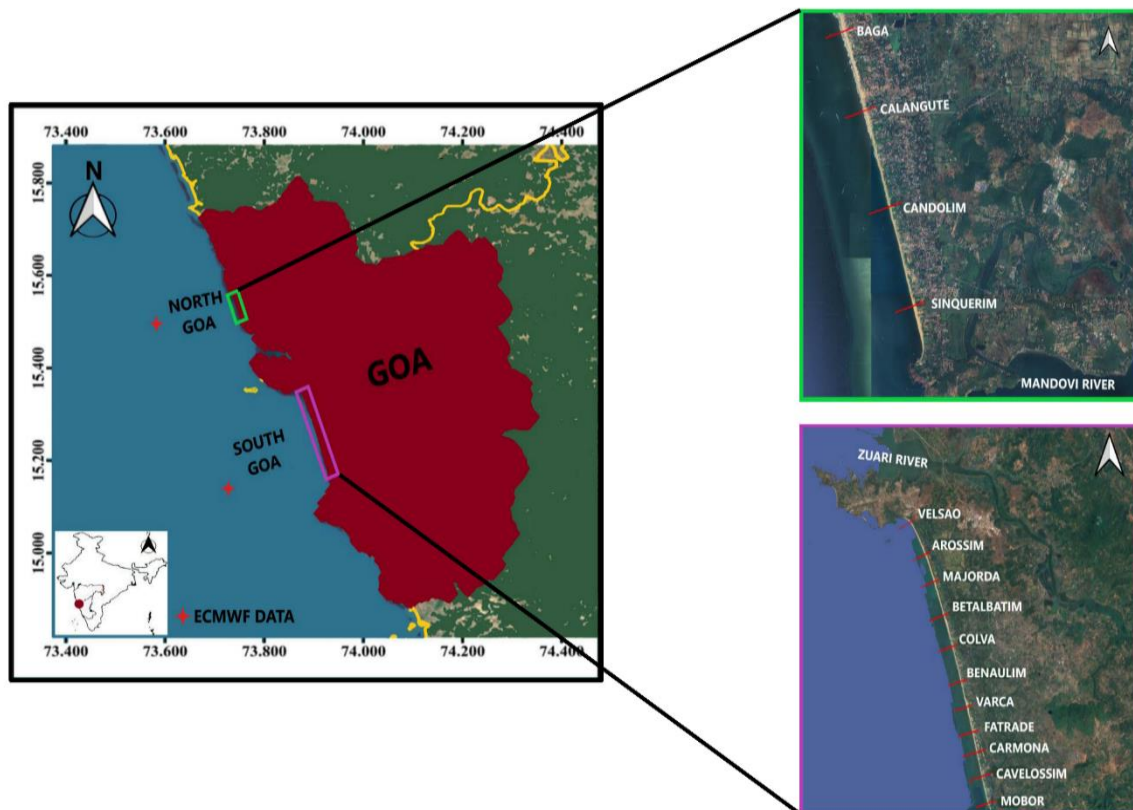
STUDY AREA AND DATASETS

Study area

The 130-kilometre-long Goa coastal region, along India's central west coast, is the focus area of this study. Bars, spits, headlands, estuaries, bays, and notable beaches have developed throughout the coastline, which stretches between the Western Ghats and the Arabian Sea (Ahmed 1972; Nadaf 2019). Fundamental morphological groups include a vast stretch of lowlands next to the coastal plain, low dissected denudational hills and tablelands to the east, and severely dissected high Western Ghats denudational hills covering the district's eastern half (Kunte et al. 2014a). Precambrian and Cuddapah rocks, Sahyadri high plateaus, and the Dharwars (quartzites, meta-greywackes, and banded hematite quartzite) are among their geological features (Wagle 1993). A significant sand-dune belt distinguishes the coastal Sahyadri high plateaus, which characterise the coastline with gentle slopes broken by crusts and troughs resulting from wind and wave action

(Wagle 1993; Wilson et al. 2014; Nadaf 2019). They are composed primarily of reddish-brown sand and lateritic soil from the Quaternary period (Aparna et al. 2005). Seasonal rivers drain the region's considerable monsoon precipitation. Goa's climate is tropical and humid (Chempalayil et al. 2014). Southwest, northeast, and pre-monsoon monsoons (SWM, June-September, NEM, October-January, and PRM, February-May) monsoons (SWM, June-September, NEM, October-January, and PRM, February-May) (Sanil Kumar et al. 2006; Dwarakish et al. 2009; Anoop et al. 2015; Fernandes et al. 2018). The southwest monsoon winds produce precipitation with an annual average of 250-300 cm (Niraj et al. 2015). The region's temperature fluctuates from 20°C to 37°C (Yadhunath et al. 2022). During the SWM, the wind blows from the southwest and the waves last between eight and ten seconds (Shanas and Sanil Kumar 2014). This coastline's beaches are characterised by a vast shoreline with steep ends, supported by well-developed dunes in some sections and collapsed dunes in others with significant ecotourism (Mascarenhas 1998, 1999). The region gets semi-diurnal tides with tidal ranges between 2 and 3 metres and a meso-tidal range of 2.3 metres (Veerayya et al. 1981).

Data and Analysis



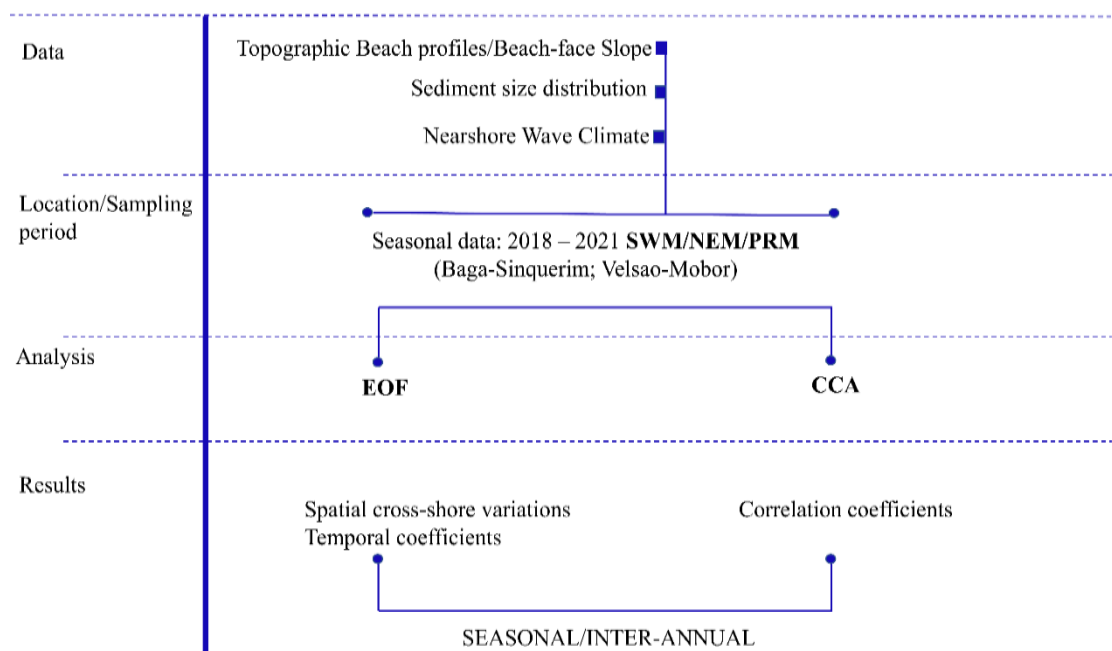
Fifteen open coast beaches in North and South Goa (Fig. 1) have been profiled, and their seasonal datasets are examined in this study. The North Goa (NG) coastal stretch consists of four main beaches

viz; Baga (BAG), Calangute (CAL), Candolim (CAN), and Sinqerium (SINQ), bound by the Baga river at the north, the headland Aguada to the south, and the Arabian sea to the west. Similarly, the South Goa (SG) stretch of semi-embayed beaches, bound at the proximal and distal axis by a prominent headland and the Sal River, comprises the Velsao (VEL), Arossim (ARO), Majorda (MAJ), Betalbatim (BET), Colva (COL), Benaulim (BEN), Varca (VAR), Fatrade (FATR), Carmona (CAR), Cavelossim (CAV), and Mobor (MOB) beaches. The individual locations of these beach profiles are essential to consider when examining their corresponding volumetric change in seasons.

Figure 1 —Map of Goa coast (insert Indian Map) showing the studied sections. Sampling stations; Top right: North Goa (NG) beaches. Bottom right: South Goa (SG) beaches.

All investigations were carried out under a broad range of wave conditions in representative months to extract information relating to SWM (July), NEM (November) and PRM (April) between July 2018 and July 2021, and geospatial locations (latitude and longitude) was assigned for each sampling location along with the sediment sample and survey location. The details of the methodology are illustrated in Fig 2.

Figure 2 —Methodology flow chart



METHODOLOGY

Single profile transects were selected for each site depending on the beach's length and accessibility. The topographic beach profiles (Fig 3) were obtained using the Leica Total Positioning System (TPS) tied to local benchmarks during the spring low tides to describe shore-normal transects between the backshore and the water line following the Emery method of beach profiling (Harley et al. 2011). Beach face slopes (β in degrees) and volume (cm^3) were estimated using a graphical method using PROFILER 3.1 (Cohen 2015). The slope is estimated by adjusting a straight line to the beach face segment of each profile at the mid-tide level reference ("reference point") as described by Bascom (1951).

Sediment Sampling and Analysis

Following Bascom's (1951) description of a "reference point" on the beach face, samples of the top 2 to 5 centimetres of beach sediments are taken at the mid-tide line, between the high and low tide lines. To remove organic and inorganic components, the samples were disaggregated with 10% hexametaphosphate and treated with 30% hydrogen peroxide (H_2O_2) and 10% hydrochloric acid (HCl), respectively, after drying at 65°C . Using the cone and quarter procedure, 100 g of treated sand was taken from each sample. The processed samples are sieved for 15 minutes using a mechanical sieve shaker with seven different sizes of ASTM sieves No. 10, 18, 35, 60, 120, 230, and 450.

This analysis seeks to identify the representative grain size showing the most significant correlation with the beach face modification across seasons. Therefore, the D_{10} , D_{50} , and D_{90} grain size percentiles were extracted from the grain size distribution. Additionally, the role that sediment gradation or sorting played in the beach face modification was also investigated. Sediment gradation Index or sorting ratios of D_{84}/D_{16} and D_{90}/D_{10} were also extracted from the grain size distribution analyses. Folk and Ward's (1957) logarithmic (original) graphic measures using the GRADISTAT® package (Blott and Pye 2001a) and The G-STAT tool (Dinesh, 2009), which are grain size distribution and statistics packages are used to extricate these parameters and to interpret other statistical measures - sorting, skewness, and kurtosis, of these sieve fractions.

Grain size information for sediment distribution is explained using millimetres (mm), as proposed by Krumbein (1934).

$$d = 2^{(-\phi)}$$

(1)

where,

$$\phi = -\log_2 d = -\left[\frac{\log_{10} d}{\log_{10} 2}\right]$$

(2)

where ϕ is particle size in ϕ units and d is the diameter of the particle in mm.

The sediment statistical parameters are then calculated thus:

Sorting or Inclusive Standard Deviation, $(\sigma) = \frac{\phi_{84} - \phi_{16}}{4} + \frac{\phi_{95} - \phi_5}{6.6}$

(3)

$$\text{Skewness, } (S_K) = \frac{\phi_{84} + \phi_{16} - 2(\phi_{50})}{2(\phi_{84} - \phi_{16})} + \frac{\phi_{95} + \phi_{50} - 2(\phi_{50})}{2(\phi_{95} - \phi_5)}$$

(4)

$$\text{Kurtosis, } (K_G) = \frac{\phi_{95} - \phi_5}{2.44(\phi_{75} - \phi_{95})} \quad (5)$$

Empirical Orthogonal Function Analysis (EOF)

The empirical orthogonal function analysis (EOF) or principal component analysis (PCA) studies spatial and temporal patterns of variation in datasets. EOF analysis is a valuable technique for discovering prevalent patterns of variability in data sets, particularly in coastal systems where responses to many processes operating at distinct temporal and spatial scales are intertwined within a single observation set. Variability patterns are typically expressed by solving the eigenvalue problem on a covariance matrix produced from the data, where each column represents a location, and each row reflects an observation time (Miller and Dean 2007; Conlin et al. 2020). The effectiveness of this strategy's prediction depends on the range of observed behaviour and varies by location.

This study employs EOFs to detect prominent spatial and temporal variation patterns in data sets from North and South Goa in India's central west. Raw data sets or demeaned data are often utilised in EOF analysis. When applied to raw data, as in this study, the first eigenfunction, often known as the mean beach function, corresponds to the mean cross-shore profile (Winant et al. 1975; Karunaratna et al. 2012b). Because the EOF method is built without any prior notions about the physical world, the eigenfunctions it produces are abstract and cannot be applied to actual problems. The observations may be physically explained with more data. If, for instance, the correct eigenfunction explains the great majority of changes, this indicates a connection to the prevailing physical process.

Because the original data used in this study were time series of beach-face slope data, the generated eigenfunctions, $e_n(x)$, reveal patterns of beach-face variability and a corresponding set of temporal

coefficients, $c_n(t)$. The profile elevation is represented by the function $h(x, t)$ as a linear combination of a few spatial and temporal eigenfunctions (and their corresponding eigenvalues):

$$h(x, t) = \sum_{n=1}^N c_n(t) \cdot e_n(x) \quad (6)$$

Variability is determined by the proportion of the data's mean squared value that each eigenfunction can explain. Since this investigation's data sets were not normalised before EOF analysis, the first eigenfunction, $e_1(x)$, is relatively near to the statistical mean. This study's substantial beach-face slope variability during each season is known as the "mean beach-face slope." Large low-frequency temporal oscillations are regularly found in $e_1(x)$, which $c_1(t)$ describes. Lower-level eigenfunctions represent the primary modes of variability over the "mean beach-face slope," whilst the remaining modes represent an ever-decreasing proportion of the total variability.

Nearshore Parameterisation

It is challenging to parameterise the nearshore environment due to the intricacy of beaches. Therefore, it is necessary to comprehend the hydrodynamic, morphological, and sedimentary characteristics of the nearshore environment in order to describe it accurately. Using ECMWF wave parameters that characterise shallow-water wave conditions, the hydrodynamic environment is presented in this paper. The median sediment diameter (D_{50}) and sediment settling velocity (w_s) give crucial morphological and geological information. To characterise the nearshore environment, applying a variety of dimensional and non-dimensional combinations of these prominent factors is typical.

Nearshore waves

The Arabian Sea bulk wind fields and offshore wave parameters (offshore significant wave height (H_o), wave period (T_p), and mean wave direction) are provided using a global wave hindcast model, ECMWF Reanalysis V5 (ERA5). The nearshore wave parameters are calculated from hourly averages of the bulk characteristics during the investigation. However, wave refraction could not be considered because the earlier wave data sets lacked angle information. Compared to measured equivalents, the ERA5 datasets yield positive results (Glejin et al. 2013; Shanas and Sanil Kumar 2014).

Waves in shallow water are depth-restricted (Mahmood and Abdullah 2016). As surges approach shallow water, they will sense the bottom and slow down. When orbital velocities grow towards the shore and surpass the wave phase speed, which decreases in the landward direction, breaking waves develop. The onward wave is overtaken by waves approaching from behind, and when it reaches a particular depth, known as critical height, the bottom's frictional resistance causes the crest to roll

over (Noujas et al. 2018). The relationship between the breaking water depth (h_b) and the breaker wave height (H_b) is represented by the following equation:

$$\gamma_b = H_b/h_b = 0.78 \quad (7)$$

Where γ_b is the breaker index.

However, because waves are irregular and unpredictable in nature, root means square wave height (H_{rms}) is a preferable means for defining nearshore wave height (Joevivek et al. 2018). Wave heights in the surf zone are depth-limited, meaning they have a nearly linear relationship with water depth. Consequently, the expression by Komar and Gaughan (1972) links H_b with H_{rms} :

$$H_b = H_{rms} = 0.39g^{1/5}(TH_o^2)^{2/5} \quad (8)$$

where T is the wave period, and H_o is the offshore significant wave height.

Wave Energy

Local wave energy is one of the most apparent indicators of beach change in coastal regions. (Berg-Sørensen and Flyvbjerg 2005) assert that as the bathymetry along the beach becomes shallow, the wave energy varies due to refraction, diffraction, and reflection. On these beaches, climate and wave energy cycles are predicted to cause the beach face to erode during monsoon conditions, when the waves are at their peak, and to build up during periods of relative calm and low wave energy, assuming nearby geologic and artificial structures do not significantly impact the beaches. ERA5 data-derived properties of offshore waves are translated using linear wave theory principles to replicate nearshore wave conditions. The total energy (E) per unit area of a shallow water wave is as follows:

$$E = (1/8)\rho g \cdot H_{rms}^2 \quad (9)$$

Where wave energy (E) is expressed in Joules per square meter (J/m^2); ρ is the density of seawater (1025 kg/m^3); g is the acceleration due to gravity (9.8 m/s^2).

Wave Energy Flux

Wave energy flux, F_x , is related to the wave energy and describes the intensity or rate at which the energy is supplied to the surf zone. Wave energy flux for shallow water conditions is expressed as:

$$F_x = E \cdot C_G = (1/8) \rho g H_{rms}^2 \cdot (\sqrt{gh_b}) \quad (10)$$

where F is the mean wave energy flux ($\text{J/m}^2\cdot\text{s}$), where C_G is the wave group velocity ($= \sqrt{gh}$ using the shallow water approximation), h_b is the water depth at breaking, substituted from equation (1) ($H_b/0.78$).

Dimensionless Fall Velocity

The parameter of non-dimensional fall velocity is also frequently employed to characterise the nearshore environment (Gourlay 1968). It is a ratio that expresses, in proportion to the wave period T_p , how long a particle with settling velocity w_s remains suspended under the influence of a wave of height H_b (substituted by H_{rms} in equation 8).

$$\Omega = \frac{H_{rms}}{w_s T} \quad (11)$$

where the settling velocity of the particle ($\text{m} \cdot \text{s}^{-1}$) is expressed as:

$$w_s = \frac{d^2 g (\rho_s - \rho)}{18 \nu} \quad (12)$$

Where ν is the dynamic viscosity of the seawater ($1.09 \times 10^{-3} \text{ kg m}^{-1} \text{ s}^{-1}$ at 20°C), ρ_s is the density of the sediment particle ($2650 \text{ kg}\cdot\text{m}^{-3}$), and d is the sediment diameter. According to Gourlay (1968) and Wright and Short (1984), the relationship between beach slope and sediment particle size represented by Ω is said to be indicative of dissipative ($\Omega > 6$), reflective ($\Omega < 1.5$) or intermediate ($1.5 < \Omega < 6$) beach states.

Canonical Correlations Analysis (CCA)

Canonical Correlation Analysis (CCA) is utilised to determine intercorrelations in bivariate datasets. In several global studies (Larson et al. 2000; Reeve et al. 2016; Hegde et al. 2022), CCA has been used to study interactions between changes in beach profile and wave conditions. Prior to CCA, it was usual practice to progressively apply the EOF approach to each of the two datasets to get filtered data sets. Using equation (1) to determine the EOF expansion, trimming the series, and reformatting the dataset, a regression matrix representing the correlation between the dominant established patterns in the two variables is generated between the two original data sets, Y , (predictor - matrix size: $nt.ny$), and Z . (predictand - matrix size: $nt.nz$). In other words, if Y is known for some time in the future, the regression matrix can be used to predict Z (Larson et al. 2000). Therefore, the predictions, Z_p , given a forecast matrix Y_p is given as:

$$Z_p = Y_p A \quad (13)$$

where A reflects the association between the two variables based on historical data.

In numerous investigations, Karunarathna et al. (2012a, 2015a) employed equation (2) as the foundation for a data-driven forecasting technique for shoreline morphology based on future wave conditions. It should be feasible to associate the temporal eigenfunctions of modes with a physical correlation to the local conditions by employing some of the typical features used to define the nearshore environment.

This work employs CCA analysis to build a regression matrix for each season's beach-face slope(predictand), with the five nearshore parameters: root means square wave height (H_{rms}), wave period (T), wave energy (E), wave energy flux (F_x), dimensionless fall velocity parameter (Ω), and five sediment parameters ($D_{10}, D_{50}, D_{90}, D_{90}/D_{10}, D_{84}/D_{16}$) as predictors. Prior to the CCA analysis, the data sets for each case were pre-filtered using EOF expansion and truncation. The CCA is used to identify the representative grain size and nearshore parameters that will likely control the beach face modification.

RESULTS AND DISCUSSION

Beach Morphology

Beach profiles of 15 sandy beaches (Fig. A1) were surveyed seasonally along the coast of Goa for the four years in focus. The slope of these seasonal profiles is calculated by linear curve fitting respectively to depict the representative beach-face slope (Table 1; Fig 3). The spatial distribution of the beach-face slope (Fig. 4) indicates that during SWM, the beach-face slope ranges from an average of 2° to 7° along the NG stretch of beaches, with the mildest beach-face slope of 0.79° (2021) occurring in the BAG, and the steepest slope of 10.36° (2020) in CAL. SG beaches are characteristically low-gradient in this season (2° to 4°), except in VAR and BET, with an average of 5° and 7° respectively.

During NEM, a slight reduction in the beach-face slope of the NG beaches (4° - 5°) is observed, except in BAG where the slope increases (4°). Similarly, in SG beaches, the beaches are relatively stable within the average range of 2° - 5° . Consequently, PRM beach-face slopes for NG are mild within the range of 2° - 6° with the mildest at BAG with an average of 0.62° (2021) and the steepest at CAL and CAND having slopes of 9° in 2020.

Similarly, marked seasonal transitional sequences are however revealed in the volumetric beach results (Table 2; Fig 3), where it is observed that there is a substantial volumetric increase during NEM when compared to the other seasons.

Table 1 —Calculated Beach-face slopes (β in degrees) for the North and South Goa Beaches

	SW monsoon					NE monsoon				Pre-monsoon			
	2018	2019	2020	2021	Avg.	2018	2019	2020	Avg.	2019	2020	2021	Avg.
North Goa													
BAG	4.05	3.66	1.69	0.79	2.55	3.58	3.11	5.96	4.22	5.87	1.21	0.62	2.57
CAL	3.63	7.79	10.36	8.25	7.51	4.10	3.54	4.39	4.01	3.91	6.33	4.73	4.99
CAN	3.90	7.66	7.79	4.40	5.94	3.51	2.66	7.03	4.40	5.09	9.55	4.09	6.24
SINQ	4.77	3.37	6.72	8.08	5.74	6.56	3.94	6.36	5.62	5.97	9.08	2.36	5.80
South Goa													
VEL	6.09	3.11	2.08	1.52	3.20	1.64	2.72	1.58	1.98	5.40	4.25	4.50	4.72
ARO	7.75	3.77	4.42	1.94	4.47	2.26	5.44	2.92	3.54	6.29	6.71	5.45	6.15
MAJ	5.44	3.11	2.99	1.72	3.32	2.10	1.89	1.17	1.72	7.79	7.19	3.40	6.13
BET	6.67	5.58	8.29	6.04	6.65	4.36	4.23	2.24	3.61	3.05	3.27	4.45	3.59
COL	2.14	2.24	4.78	2.49	2.91	4.07	2.33	1.44	2.61	3.59	4.06	2.40	3.35
BEN	3.91	2.98	4.38	2.96	3.56	4.33	2.84	2.40	3.19	2.84	2.15	2.40	2.46
VAR	3.15	4.44	3.87	9.34	5.20	6.34	5.23	5.32	5.63	2.03	2.95	2.99	2.66
FATR	4.04	3.00	1.51	2.06	2.65	3.35	2.12	5.36	3.61	1.63	3.05	2.20	2.29
CAR	2.20	3.03	2.08	2.29	2.40	3.09	2.79	1.40	2.43	1.89	3.22	2.76	2.62
CAV	2.59	6.21	4.43	1.70	3.73	7.60	3.39	3.44	4.81	2.08	4.35	2.58	3.00
MOB	1.72	2.00	3.23	2.35	2.33	0.90	3.28	1.99	2.06	2.13	4.83	2.80	3.25

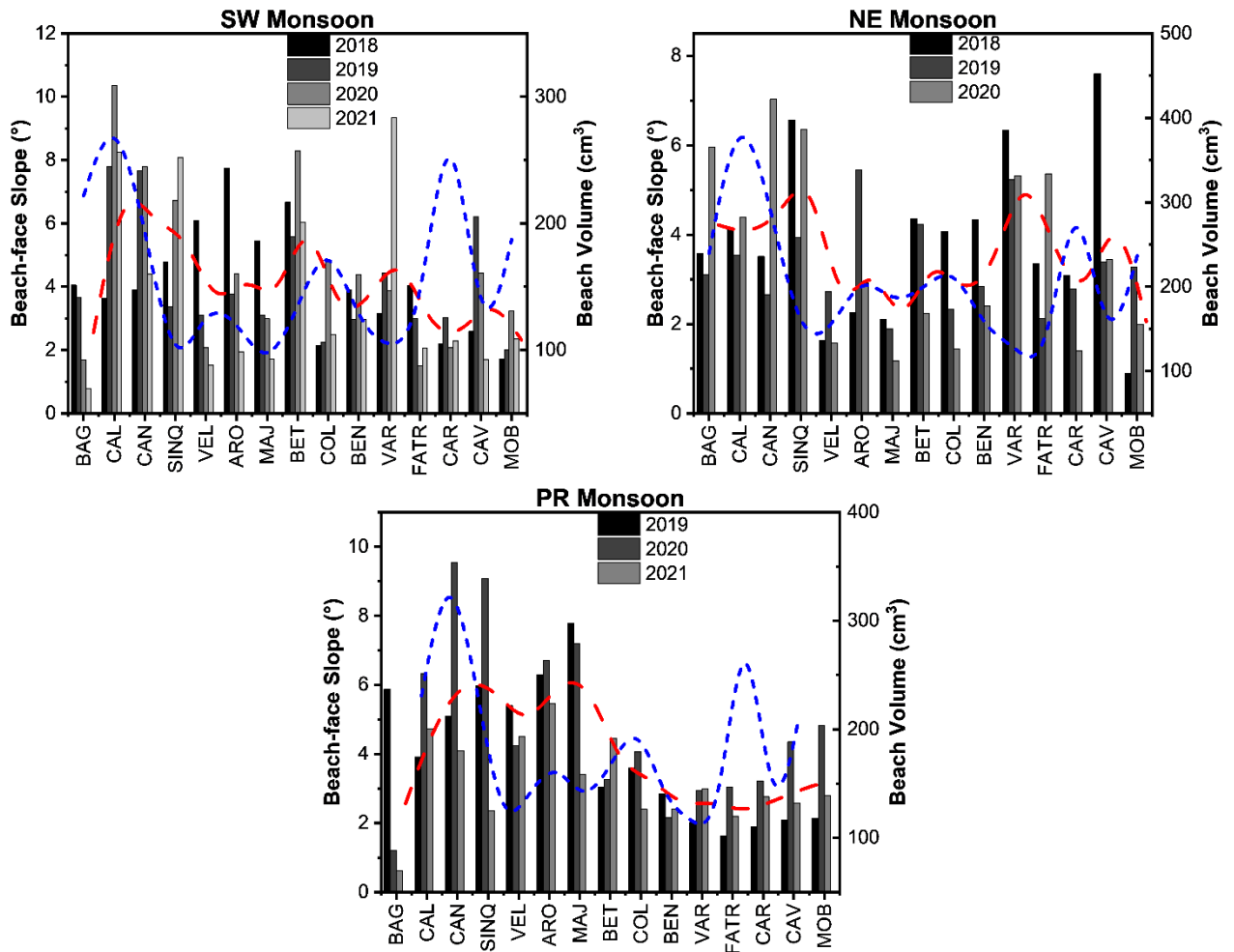


Figure 3 —Spatial distribution of Beach-face Slopes along Goa coast for SW monsoon, NE monsoon and Pre-monsoon (Red dashed line indicates the average beach-face slope, and the blue dashed line represents the average beach volume for each season)

Table 2 —Calculated Beach Volume (cm^3) for the North and South Goa Beaches

	SW monsoon				Avg.	NE monsoon				Avg.	PR monsoon				Avg.
	2018	2019	2020	2021		2018	2019	2020	2021		2019	2020	2021		
NORTH GOA															
BAG	266.3	329.8	108.2	183.4	221.9	222.4	435.8	60.9	239.7	417.7	261.4	270.9	316.6		
CAL	316.5	434.6	151.5	279.7	295.6	502.7	475.5	309.9	429.4	513.3	434.6	348.7	432.2		
CAN	263.4	372.8	47.0	107.3	197.6	321.0	371.4	199.2	297.2	454.7	146.9	134.7	245.4		
SING	79.8	179.9	22.8	8.1	72.6	78.3	242.6	74.2	131.7	249.8	75.1	68.4	131.1		
SOUTH GOA															
VEL	62.7	113.4	186.2	189.1	137.9	117.9	128.7	194.3	146.9	207.2	252.4	201.6	220.4		
ARO	73.7	260.7	71.0	90.6	124.0	229.0	250.6	179.0	219.5	291.8	111.7	153.7	185.7		
MAJ	52.7	115.0	62.6	99.8	82.5	121.9	274.0	138.3	178.1	223.1	136.9	135.4	165.1		
BET	165.8	125.9	123.3	119.7	133.7	192.1	175.5	225.6	197.7	178.3	123.6	146.6	149.5		
COL	178.2	224.5	152.6	215.7	192.7	225.8	228.7	231.6	228.7	254.2	208.5	290.4	251.0		
BEN	119.8	114.0	109.2	139.1	120.5	129.0	100.3	216.5	148.6	80.8	226.4	196.5	167.9		
VAR	164.2	89.2	96.8	46.4	99.2	178.7	150.3	61.5	130.2	200.9	139.1	117.8	152.6		
FATR	81.2	108.1	149.3	120.2	114.7	86.9	136.3	53.1	92.1	187.7	172.9	174.0	178.2		
CAR	310.5	301.7	382.0	316.4	327.7	325.0	494.8	249.5	356.4	429.9	401.9	471.8	434.5		
CAV	121.8	75.3	44.6	90.7	83.1	105.8	57.0	141.1	101.3	179.3	120.0	133.0	144.1		
MOB	302.1	216.0	120.3	111.1	187.4	226.1	285.6	197.9	236.5	389.1	284.6	153.7	275.8		

Empirical Orthogonal Functions (EOF)

The work's high point is to utilise EOFs to analyse seasonal beach profile records with an emphasis on the beach face slope. EOF analysis demonstrated the spatial and temporal variation in beach-face morphology. According to the "rule of thumb", three to five EOF modes should account for the majority of the variability in a dataset. As the number of modes increases, the overall variance in the datasets decreases; this is sometimes known as "noise."

Table 3 illustrates the variation in beach face slope induced by the EOF analysis in three modes extracted to explain the eigenvalues, percentages of variance, and cumulative variance contributions explained by the top three eigenfunctions that dominate the beach face changes at the locations. According to the findings, the first three eigenfunctions account for about 99% of the seasonal data fluctuation. In Fig. 4, the initial three spatial and temporal variability forms are enumerated, explaining most fluctuations (75-80%) for all seasonal beach profiles analysed. According to Winant et al. (1975), the Eigenfunction $e_1(x)$, also known as the "mean beach function," reflects the "mean beach-face slope". The data's time regularity - temporal coefficients - $c_1(x)$ also produced accurate results and permitted consistent physical interpretation of EOFs.

Table 3 —Eigenvalues and variances explained by the first three modes.

		$e_1(x)$	$e_2(x)$	$e_3(x)$
SWM	Eigenvalue	6.23	5.38	3.39
	% Variance	41.52	35.88	22.59
	Cumm. % Variance	41.52	77.4	100
NEM	Eigenvalue	7.5	4.75	2.75
	% Variance	50	31.67	18.33
	Cumm. % Variance	50	81.67	100
PRM	Eigenvalue	8.46	5.15	1.39
	% Variance	56.37	34.33	9.29
	Cumm. % Variance	56.37	90.71	100

SW Monsoon

In Fig. 4, the first spatial eigenfunction $e_1(x)$ mode demonstrates significant fluctuations across the beaches. Negative amplitudes from lower gradient slopes predominate on the NG beaches, except BAG, whilst positive and negative values alternated on the SG beaches. The temporal eigenfunction $c_1(t)$ yielded positive amplitudes in 2018 and 2019; however, 2020 and 2021 exhibited a substantial decline. In its mean condition, the combination of $c_1(t)$ and $e_1(x)$ indicates alternating slope buildup and collapse stages. While Table 3 indicates that the cross-shore process dominates variability in this

region with a contribution value of 41.5%, the sign of $c_1(t)$ influences $e_1(x)$, the time-factored modulation of the beach-face slope.

Spatial diversity is depicted in Fig. by $e_2(x)$ with a 35.8% variance (Table 3). Significant variations were also captured by the time evolution of the second eigenfunction along the beach characteristics (Figure 4c).

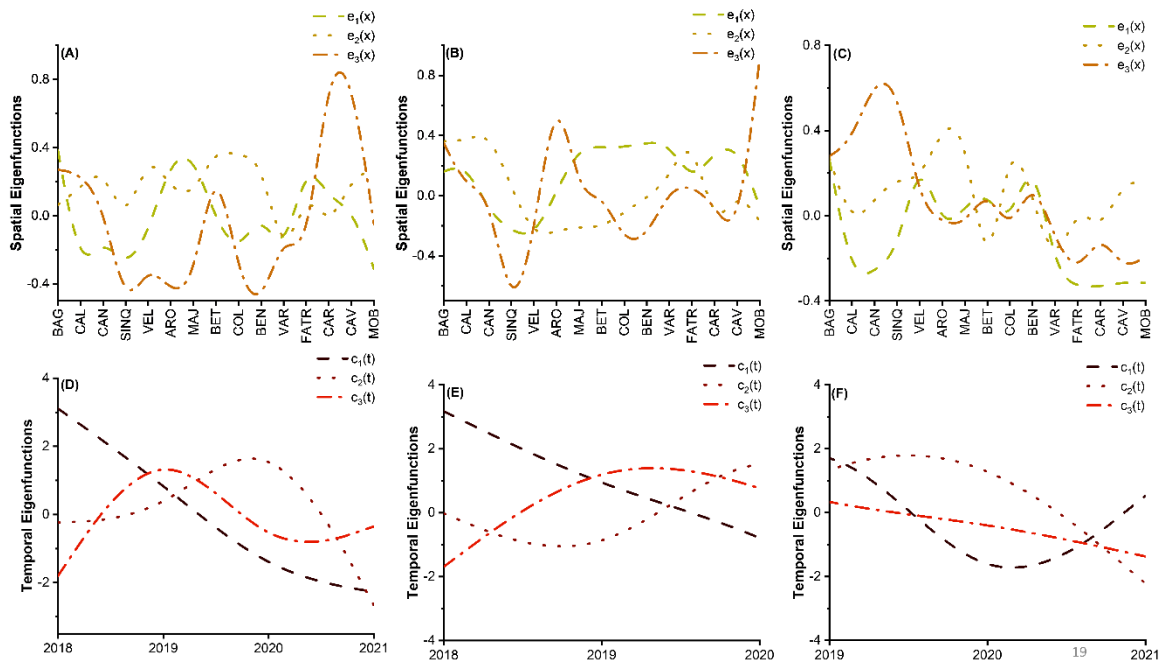


Figure 4

—Spatial plots of Empirical orthogonal functions (top panel) and their Temporal coefficients (bottom panel) for SW monsoon (A and D), NE monsoon (B and E), and PR monsoon (C and F)

While specific beaches are consistent, as seen in Figure 4b, most beaches are variable. Positive amplitudes are observed for slope amplitudes that increase relative to the mean slope $e_1(x)$ in the spatial eigenfunctions CAL, CAN, VEL, BET, COL, and MOB, whereas the opposite is true for CAR. The other beaches were highly stable. The values of $c_2(t)$, the first temporal mode, are depicted in a different pattern from $c_1(t)$, with continual alterations between 2018 and 2020. The behaviour of the first mode is similarly reflected by the combination of $e_2(x)$ and $c_2(t)$. The third mode, $e_3(x)$, had minor spatial eigenfunction variability (22.6%), with no distinct variation from the preceding mode. Similarly, the temporal coefficient $c_3(t)$ exhibited slight variation.

NE Monsoon

This season, the first eigenfunction, $e_1(x)$, accounts for 50% of the observed variance. The beaches had predominantly positive amplitudes, as shown by $e_2(x)$ (32%; Table 3), but the bulk of changes in 2018 and 2019 have negative amplitudes, as shown by $c_2(t)$. Moreover, the variability of the third mode contributes approximately 18% to change. Similar to the first and second modes, specific beaches undergo alterations. However, the extracted modes in the datasets BAG, CAL, VAR, and FATR are stable.

PR Monsoon

The first spatial function illustrates the slope rise in BAG, VEL, MAJ, BET, and BEN, accounting for 56.37 % of the total variance. On the remaining beaches, one can observe negative amplitudes. The first function's temporal evolution is positive between 2019 and 2021 and negative in 2020. The second spatial function (34% variance) has the opposite shape of the first function with larger positive amplitudes. Its temporal development exhibits a similar pattern, with positive amplitude in 2019 and 2020 and negative amplitude in 2021. The third spatial function, which accounts for less than 9 % of the variance, has mild rhythmic behaviour across the beaches, especially along the SG stretch, and the temporal function reflects this. There is no visible effect of the reconstructed spatial eigenfunctions on the optimal slopes of BAG, VEL, BEN, VAR, and CAR.

Wave Climate and Nearshore conditions

Wave information for the study region was generated using ECMWF (ERA5) data from two nodal locations 25 kilometres off North and South Goa beaches (Table 5). Using equation (9), the breaking wave energy and flow were calculated as a function of H_{rms} based on the ECMWF dataset. The sea wind influences the seasonal variation in offshore significant wave height (H_o) measured in the research area. H_o ranged between 0.8 and 0.9 metres, and the waves were north-northwesterly during the PRM (Figure 4). During the southwesterly directed waves of SWM, H_o rises and peaks between 2 and 3 m, frequently accompanied by episodic cyclonic occurrences (Figure 5). H_o readings ranged from a minimum of 0.8 m in NG to a maximum of 2.9 m in SG during the NE monsoon.

Similarly, the wave period (T_p) along the beaches of NG and SG was a maximum of 7.6 seconds during PRM, 8 to 9 seconds during SWM, and 6 seconds during NEM. Except for tropical storms associated with the southwest monsoon, the mean wave energy and wave energy flow in the study area are moderate. Compared to the SWM months, the PRM and NEM months have a relatively calmer wave climate. This alteration is anticipated to affect the seasonal fluctuation in silt distribution along the coast of Goa.

Table 4 —Nearshore parameters for North and South Goa for the years 2018 to 2021

			H_o	T_p	H_{rms}	E	F	D_{50}	w_s	Ω	
NG	2018	SWM	3.06	9.37	3.69	4628.80	31501.98	0.35(M)	0.10	4.01(I)	
		NEM	0.69	6.80	0.99	1242.98	4383.61	0.29(M)	0.07	2.16(I)	
	2019	PRM	0.92	7.09	1.26	1585.58	6315.67	0.23(F)	0.04	4.14(I)	
		SWM	2.67	9.14	3.27	4108.42	26341.94	0.25(M)	0.05	6.99(D)	
		NEM	0.86	7.34	1.21	1519.90	5927.34	0.25(M)	0.05	3.21(I)	
		2020	PRM	0.90	7.63	1.28	1603.68	6424.12	0.29(M)	0.07	2.43(I)
		SWM	2.34	9.15	2.95	3699.38	22507.55	0.38(M)	0.11	2.81(I)	
		NEM	0.79	7.40	1.13	1424.71	5379.28	0.25(M)	0.05	2.98(I)	
	2021	PRM	0.89	7.54	1.25	1573.84	6245.65	0.23(F)	0.04	3.75(I)	
		SWM	2.49	8.40	2.99	3755.40	23020.74	0.38(M)	0.12	3.07(I)	
	SG	2018	SWM	0.82	7.08	1.14	1436.27	5444.88	0.20(F)	0.03	4.77(I)
			NEM	2.92	9.36	3.55	4459.66	29791.22	0.24(F)	0.05	7.86(D)
2019		PRM	0.67	6.84	0.97	1214.06	4231.50	0.21(F)	0.04	3.85(I)	
		SWM	0.87	7.31	1.22	1530.60	5990.00	0.22(F)	0.04	4.40(I)	
		NEM	2.56	9.11	3.16	3971.53	25036.41	0.25(M)	0.05	7.00(D)	
		2020	PRM	0.82	7.36	1.17	1464.82	5608.06	0.20(F)	0.03	4.87(I)
		SWM	0.87	7.79	1.25	1568.18	6211.97	0.21(F)	0.04	4.40(I)	
		NEM	2.24	9.13	2.84	3566.53	21306.09	0.24(F)	0.05	6.55(D)	
2021		PRM	0.84	7.60	1.21	1515.75	5903.03	0.20(F)	0.03	4.74(I)	
		SWM	2.37	8.41	2.88	3615.18	21743.52	0.21(F)	0.04	9.18(D)	

(*) F-Fine sand. M- Medium sand, I-Intermediate beach state, D-Dissipative beach state

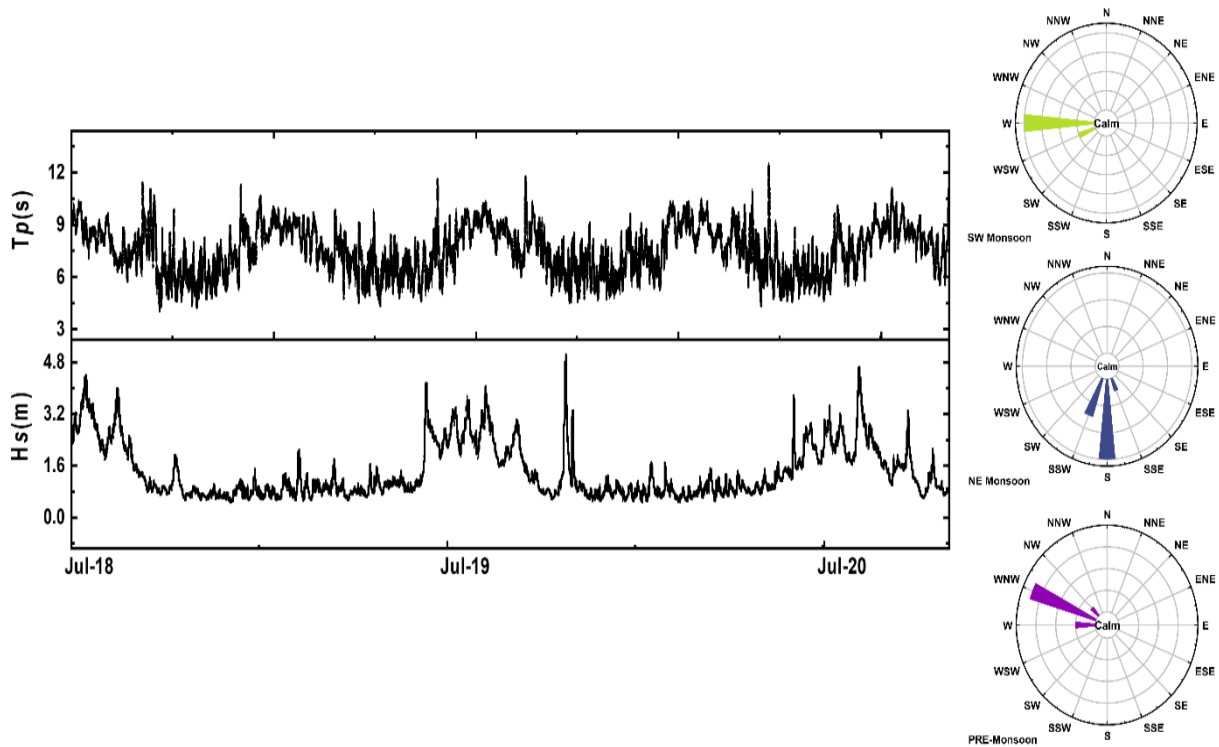


Fig. 5 —Wave properties extracted from the ECMWF database. Left panel: Offshore significant wave height (H_s) and Wave period (T_p). Right panel: Wave Direction for SW, NE, and PR monsoon seasons.

Sediment composition

Beach surface samples were analysed, and results for select sedimentological parameters were presented for each season from 2018 through 2021 (Table A1, Fig 6). Except for PRM, where medium sand (33.3% of the total composition) and fine sand (66.7% of the total composition) account for the overall composition of the NG beaches, the sediment median diameter (D_{50} ; Table 4) was wholly composed of fine sand (100%) for all years and seasons examined. Fine sand is classified as $D_{50} = 0.1\text{--}0.25$ mm, medium sand as $D_{50} = 0.25\text{--}0.5$ mm, and coarse sand as $D_{50} > 0.5$ mm. Except for the NEM, where medium sand (33.3% of reported compositions) and fine sand (66.7% of reported compositions) were observed, sediment diameters along the SG beaches were dominated by fine sand (100%).

Typically, grain-size distributions are described using three additional descriptive statistics in addition to the median grain size. Sorting, also known as standard deviation, measures the extent to which a distribution is broad or dispersed. The measure of divergence from a symmetrical (normal) distribution is skewness. Kurtosis indicates whether a distribution is skewed or flat (Blott and Pye 2001). Folk and Ward (1957) introduced the most widespread sorting measures, skewness and kurtosis, which are utilised in this research.

A gradation index or uniformity coefficient can be used to measure the homogeneity of sand. Less homogeneous sand has higher gradation index values ($\gg 1$), while more uniform or well-sorted sand has lower values (~ 1).

The standard deviation or sorting revealed varying particle dispersion in the three seasons. In PRM, moderately sorted to moderately well-sorted sands within the range of 0.29 to 1.07 dominated. A predominance of well-sorted to moderately well-sorted sands characterised the SWM (0.34 to 1.59). In NEM, the beaches revealed a dominance of moderately sorted to moderately well sorted to moderately sorted sands (0.29 to 1.41).

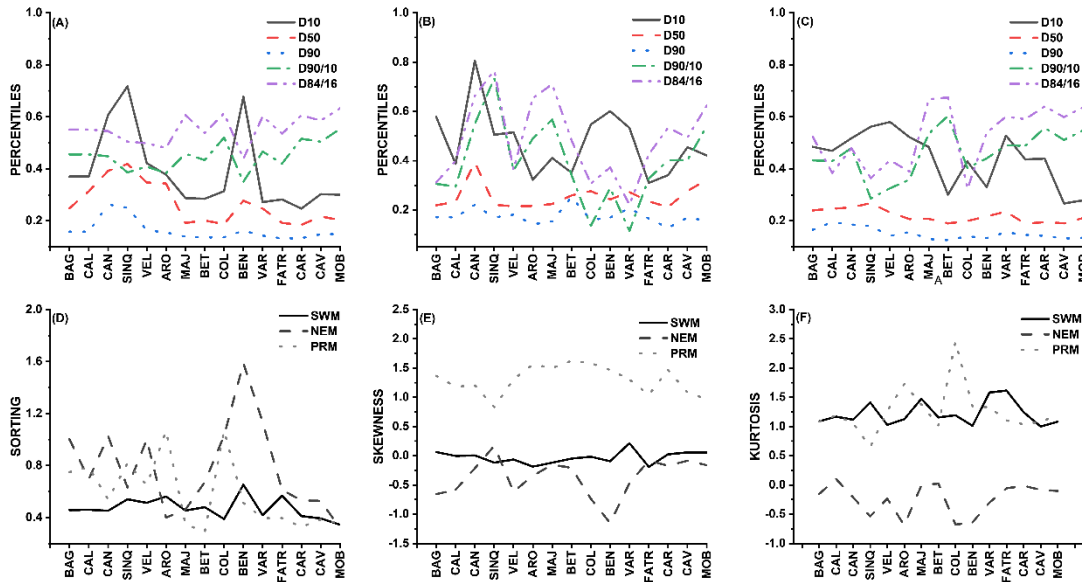
Skewness distribution for all three seasons showed marked dominance of symmetrical to very coarse skewed, with more symmetrical distributions occurring in SWM than in the other seasons.

A near symmetry in the degrees of peakedness (kurtosis) was recognised in all three seasons. Results indicate a succession of mesokurtic to leptokurtic/very leptokurtic sands in SWM and NEM. PRM showed a wide range of mesokurtic to very platykurtic sands.

Similarly, observed patterns in this measured data set demonstrated how several typical sediment parameters influenced the beach face shape. The D_{10} and D_{50} sediment sizes exhibited the most

negligible variation, with the sediment sizes not altering significantly. In contrast, the D_{90}/D_{10} and D_{84}/D_{16} sediment sorting/gradation ratios were more variable for all seasons.

Figure 6 —Sediment grain size composition for North and South Goa beaches. Spatial distribution of



sediment grain size percentiles (top panel) for SWM (A), NEM (B) and PRM (C); Spatial distribution of sediment grain size statistical parameters (bottom panel): sorting (D), skewness and kurtosis (F).

Dimensionless fall velocity of sediments (Ω)

Except for SWM 2019, when the beaches were dissipative, the dimensionless fall velocity of sediments (Ω) on the NG beaches was predominantly within the moderate range (Table 4). During SWM and PRM, the SG stretch of beaches tended to be in an intermediate beach state, whereas dissipative beach states dominated during the NEM season.

Canonical Correlations (CC)

CCA was utilised to investigate the statistical relationship between root means square wave height (H_{rms}), wave period (T), mean wave energy (E), wave energy flow (F_x), dimensionless fall velocity (Ω), sediment parameters, and beach-face slope. By analysing the CCA's seasonal performance, 15 beach-face slopes were utilised for each season from July 2018 to July 2021 to generate variability regression matrices.

The needed beach-face correlations were calculated using these variability regression matrices and the EOFs for H_{rms} , T, E, F_x , Ω and environmentally sensitive sedimentary parameters (D_{10} , D_{50} , D_{90} , D_{85}/D_{16} , D_{90}/D_{10} , mean, sorting, skewness and kurtosis). During the CCA, the remaining 5% were interpolated as noise using an EOF threshold of 95%. Following the application of north's rule of thumb, it was determined that the sampling errors of the eigenvectors obtained by the EOF method were modest, demonstrating the validity of this assumption (North et al. 1982). The squared values of the canonical variate pairs (Table 5) are comparable to r^2 values in their interpretation, with values above 0.7 considered significant.

Table 5 — Canonical correlations (CC) and Squared Canonical correlations (SQ. CC) of beach face slope with nearshore parameters

		H_{rms}	T	E	F_x	Ω	D_{10}	D_{50}	D_{90}	$D_{90/D_{10}}$	$D_{84/D_{16}}$	Sd	Sk	Kurt
SWM	CC	0.77	0.89	0.77	0.77	0.59	0.28	0.04	0.50	0.86	0.86	0.87	0.88	0.95
	SQ. CC	0.60	0.79*	0.60	0.59	0.35	0.08	0.00	0.25	0.74*	0.74*	0.76*	0.78*	0.90*
NEM	CCA	0.99	0.96	0.57	0.79	0.55	0.06	0.17	0.99	0.99	0.97	0.98	0.99	0.99
	SQ. CCA	0.98*	0.92*	0.33	0.62	0.31	0.00	0.03	0.98*	0.99*	0.95*	0.97*	0.98*	0.98*
PRM	CCA	0.46	0.58	0.14	0.50	0.69	0.61	0.75	0.52	0.36	0.46	0.40	0.42	0.46
	SQ. CCA	0.21	0.34	0.02	0.25	0.48	0.38	0.56*	0.27	0.13	0.21	0.16	0.18	0.21

(*) - significant correlation values

Variations in the performance of CC of the beach-face slope with nearshore and sedimentologic parameters across a four-year computing period revealed substantial squared canonical correlations (Table 5). During SWM, T , $D_{90/D_{10}}$, $D_{85/D_{16}}$, sorting and skewness have significant correlations of 0.79, 0.74, 0.74, 0.76, and 0.78, respectively, while kurtosis had the most significant value of 0.90. During the NEM, significant squared CC was observed in all sedimentologic parameters except D_{10} and D_{50} , with the most negligible correlations (0.00 and 0.03). During the PRM, only CC with sediment D_{50} was significant (0.56). The result indicates poor coherence between the beach face slope and the percentiles D_{10} and D_{90} when CCA is computed; hence, they cannot be used to evaluate beach-face slope modification.

Assessment of Nearshore Coastal Processes on Beach-face Morphodynamics

The wind waves approaching the Goa coast during the NE and SW monsoon are unidirectional and energetic, trending from the northeast and southwest directions, respectively (Fig. 5). The incident wave characteristics on India's Central West Coast strongly influence littoral transport and beach modification (Wagle 1993; Seelam et al. 2014). The strength of the incoming wave field significantly influences the variety of beach profile forms observed along the coast of Goa. Even though wave breaking angle was unavailable for examining the effects of wave direction on beach slope alteration, the variation in beach profile shape shows that the local wave field is primarily responsible for beach modification. The seasonal variation of H_{rms} , E , and F_x (Table 3) indicates that wave properties are more significant during the SWM, less during the NEM monsoon, and moderate during the PRM on the NG coast. In SG, there is a distinct pattern where the wave parameters significantly peak during NEM and moderate in the other three seasons. The effect of the wave field is further reflected via significant sediment transfer evident in the volumetric increase recorded in NEM, particularly for SG beaches.

Similarly, volumetric indices (Figure 3) demonstrate that hydrological conditions and sediment transport cause seasonal oscillations on the beaches. Table 2, which provides volumetric data, shows that the shoreline accumulates more sediment during the NEM than during the SWM and PRM. This illustrates a seasonal wave action process that causes the exchange of beach-face sediment. These results (Table 1; Fig 3) indicate that waves during these two monsoons can transfer sediments in the cross-shore direction, thereby altering the slope, and the findings corroborate prior research that identified the NE and SW monsoons as the primary drivers of beach morphology changes along the Indian coastline (Jayakumar et al. 2001; Chempalayil et al. 2014; Seelam et al. 2014; Kunte et al. 2014b).

The seasonal sediment characteristics of Goa's two extremes varied with fine to medium sand. Bujan et al. (2019) discovered a correlation between sediment grain size and beach-face steepness, with larger (smaller) particles correlating to a steeper (flatter) beach face. According to the statistics, most SG beaches have low slopes throughout the year compared to the NG beaches (Table 1; Fig 3). The strong headlands and neighbouring estuaries that divide the NG and SG lengths give some physical parallels but also a striking contrast that variances may explain in site characteristics (the SG coast is an embayment while the NG coast is an exposed beach stretch). Sediment D_{50} is around 0.20 mm in SG and approximately 0.3 mm in the NG region. The median sediment diameter of the open coast NG beaches and medium sands were significant during SWM and NEM, while fine and medium sand fractions dominated during PRM (see Fig 6). Due to the minuscule particle sizes, capillary forces maintain the beach's moisture for a significant portion of the time (Fredriksson et al. 2017), allowing it to maintain its shape for the most part. This is consistent with the significant wave energy regime seen for SWM, indicating that fine sands were likely removed by the backwash's turbulent action, leaving medium sands behind (Folk and Ward 1957a; Blott and Pye 2001a). The reverse is the case in SG, where the wave energy flux during NEM is substantially greater than that during SWM, significant enough to deposit both fine and medium sands. Hence it can be surmised that the seasonal effects of the NEM climate can be considered a stimulant for sediment transport, volume variations, and slope change on the SG beaches.

Temporal changes in sedimentology can be associated with the beach face's morphological response, despite the sedimentary signal not reflecting the regional trend of morphological change. Seasonal slope change affects sediments' coarsening and accumulation. Seasonal variations in the size and distribution of sediments have been reported. Changes in beach slopes, estuary runoff, and swash processes can also alter sediment grain composition in beaches (Reis and Gama 2010). When the morphology of a beach partially reconstructs highly active wave activity, beach erosion can occur

(Senechal and Ruiz de Alegría-Arzaburu 2020). Buscombe and Masselink (2006) found that when sediment size increased, so did slopes on beaches. Therefore, the change in slope may promote the accumulation of coarser grains.

Unlike nearshore volumetric variations, changes in sedimentology of this study's datasets do not exhibit large spatial oscillations, particularly in the median grain size; nonetheless, beach face shape may be responsible for some intriguing trends in seasonal sediment size data. The data reveal a seasonal correlation between some effective sediment grain size parameters and beach face slope. This supports recent research conducted along the Goa coast, showing that the distribution of sediments along the beaches is significantly influenced by seasonal factors (Okon et al. 2023).

Grain sorting suggests that the energy conditions of agent deposition reflect in the distribution of sediments (Friedman and Sanders 1978). The prevalence of well-sorted to moderately well-sorted fine sands (Table A1) during the SWM is consistent with Tucker (1990) who identified most sedimentary systems as having best-sorted sediments in the fine-sand size range. However, the wide range of grain sorting observed in NEM and PRM seasons (Table A1) suggests that sediments may be reworked as current and wave energy conditions change (Friedman 1967).

For all seasons, the skewness pattern is symmetrical and very coarsely skewed, with finer sand contributing progressively more sediments than coarser fractions in the direction of the energy gradient, resulting in negative skewness. The tendency to negative skewness supports Tucker's (1990) claim that well-sorted beach sands are typically negatively skewed. This is likely due to fluctuating energy levels in the transporting medium and wave energy dissipation by nearshore bars or wave-breaking zones (Duane 1964) According to Azidane et al. (2021), the symmetrical population depicts moderate energy conditions or a lack of extreme conditions, such as wave breaking, tidal variations or seasonal supply of detrital conditions. Therefore, by changing sediment transport thresholds, this seasonal variation in textural qualities may have a favourable or adverse effect on the beach face. This is feasible if a single transit event encourages sediment coarsening by removing particles. This will result in increased bed roughness due to the more significant protrusion of the larger grains remaining in the boundary layer, increased sediment mobility and preferential transport of the largest grains due to their protrusion into the boundary layer, or decreased mobility due to the higher entrainment thresholds of the coarser grains.

Variations in kurtosis (or degree of peakedness) illustrate the varied pattern of flow characteristics in a given depositional environment (Baiyegunhi et al. 2020). The intermittent mesokurtic to leptokurtic

distribution describes the sorting of matured sands transported from a higher energy environment and deposited via the continuous addition of finer fractions after winnowing (Baiyegunhi et al. 2020).

There was a substantial CCA correlation between the beach face slope and the sediment gradation/sorting ratios D_{90}/D_{10} and D_{84}/D_{16} during the NEM and the SWM. All sediment parameters showed low correlation indices during the PRM. On the other hand, the inadequate link between sediment D_{10} and D_{50} and the beach face slope supports divergent behaviour. A significant correlation with the D_{90} in NEM and SWM suggests that the beach face sediments have become coarser due to the removal of fine sediments during this season. Considering the variable nature of transport processes in conjunction with the prevailing hydrodynamics, these conclusions support those of Gao and Collins (1994). When profiles contain a sufficient quantity of coarse sediment, suspending the finer sediment fraction on the bed surface becomes crucial in lowering erodibility of the beach face.

Similarly, the intermediate states of these beaches are recorded in all seasons except for some exceptions in SG during NEM, where the beach state is dissipative (Table 4). According to Aagaard (2014), Intermediate beach states facilitate dynamic beaches and the crucial morphodynamic loop between hydrodynamic processes and morphology with effective transport rates and gradients. As a result, it is difficult to predict the complex morphodynamic behaviour of these states due to their diverse morphologies, which include more prominent subtidal features, faster transport rates, and more pronounced gradients (Senechal and Ruiz de Alegría-Arzaburu 2020).

The most significant aspect of the study was the application of EOFs to daily beach profile data sets, utilised to illustrate the observed variations in beach-face shape as a function of time and space. The data's temporal regularity gave acceptable results and allowed a consistent physical interpretation of EOFs. The three first eigenfunctions explain seasonal variation in beach-face slopes across three seasons with the largest eigenvalues. The eigenfunction with the most significant value reveals the position of the mean beach-face slope. The maximum variation beach face slope from the mean is indicated by a second eigenfunction, which in the context of this study may be referred to as the "slope increase function." This function's time dependency demonstrates annual periodicity with relation to each season, hinting that it should be linked to sand movement on or offshore and slope alteration produced by waves driven by climatic variations. The third eigenfunction with unique periodicity in time dependence tends to mimic the second eigenfunction.

According to EOF results (Figure 5), the beach slope was steepest during the NE monsoon and significantly less steep during the NEM and PRM, especially on SG beaches. Following the

observations of Reis and Gama (2010), the rhythmic volatility of the SG beaches likely indicates that the beaches seek balance via beach face/nearshore sediment transfer. The change in beach slope during the SWM likely indicates that the dominant process erodes and transports sand from the beach face to the ocean. During the NEM, however, the surging wave utilises swash action to transfer suspended sediments from the nearshore to the beach-face region and does not recover them due to the associated backwash. The PRM's softer slopes characterise periods of beach recovery. During this time, sandbars are swept from the beach and deposited in the beach-face region to build the slope. The negative EOF amplitudes observed in the variability of these beaches may also indicate significant construction and human activity on this site (Mascarenhas 1999). However, it is believed that finely spaced data collection could produce an extensive dataset to address spatial and temporal changes in beach morphology.

In order to assess the cross-correlation of the beach-face morphology and select nearshore parameters, the CCA method adopted revealed results deemed adequate and useful for evaluating the variability of beach slopes. The primary limitation of the CCA technique is that the wave data was extracted from point ECMWF data required to determine beach morphodynamics; consequently, beach-face slope positions can be more precisely predicted with sufficient accuracy using finely spaced grid wave data. The CCA's ability to offer accurate and realistic quantitative computations is constrained by the data used to generate the variability regression matrix, in this case, single-point data along the coast for four years. According to the temporal canonical mode shown with these characteristics, the beach-face slope correlates considerably with the wave parameters. Significant SWM squared CC (0.6) indicates that beach-face slope variability responds to changes in this wave climate. This view is supported by the findings of Karunarathna et al. (2015a), Reeve et al. (2016), Chatzirodou et al. (2017), Bujan et al. (2019) and Vos et al. (2020), who discovered a substantial correlation between coastal morphologic change and wave energy. Numerous other research (Larson and Kraus 1995; Larson et al. 2003; Larson and Bayram 2005, Hallin et al. 2019, Jovivek et al. 2019) have also demonstrated the usefulness of wave climate distribution and beach profiles as metrics for analysing processes and beach responses.

The findings of the CCA also illustrate the correlations between beach and nearshore factors. Positive amplitudes in the correlation between mean wave energy and wave energy flux indicate that the values of these parameters vary with beach face slope. Contrary to the findings of Bujan et al. (2019), who linked sediment grain size to slope modulation, the intermediate beach state and nearly uniform sediment grain size in this active zone have no direct impact on slope configuration, as indicated by negative amplitudes in the correlations between sediment D_{50} and dimensionless fall

velocity. Based on these observations and our findings, we conclude that the SW and NE monsoonal fluctuation of nearshore processes promotes sediment redistribution along the beach face.

Fluctuation patterns in wave and profile data appear to be amenable to identification utilising the CCA and EOF techniques. Other factors, such as coastal geomorphology and geometry, may also have a significant impact on the evolution of this region, meaning that studies such as those presented in this article provide an excellent opportunity to generate ideas for mesoscale modelling of the beach face. It is important to note that the temporal amplitudes of the nearshore parameter distributions' CCA modes and the beach face slope do not have a strong enough relationship to suggest a clear cause-and-effect relationship. This work reveals that if the wave climate is well predicted, the EOF gives reliable estimates of beach-face slope variation, and the CCA extracts different correlation patterns with nearshore characteristics that can be used to predict future beach-face placements. The findings of the EOF study also demonstrate how successfully the method captured multi-scale temporal changes in a very complex beach system subjected to various surge conditions. In addition, the approach offers the possibility of extrapolating past behaviour to predict future beach variability.

It is commonly known that high-quality monitoring data are essential for informing coastal management. It is essential to use the methods and data from short-term and seasonal research such as this one to establish pilot databases to expand our understanding of mesoscale dynamics and develop more accurate and reliable regional mesoscale models. The data-driven approaches outlined in this study and evaluated using real-world data represent only a portion of the statistical tools available to address this problem. The results of this pilot study indicate that this statistical technique has enormous potential when applied to data from Goa beach, as the generated functions demonstrate a clear relationship to natural processes.

Conclusion

This study investigated seasonal trends in the spatial and temporal variability of beach face morphology using two data-driven techniques (EOF and CCA) at fifteen different locations along the coast of Goa over four years. The current dataset consists of nearshore wave parameters, beach morphology, and sediment particle size distribution for the various monsoon seasons, assembled from comprehensive field research done between July 2018 and July 2021. Records of beach morphology and deposits provide insight into the beach's state and depositional environment. It explains how nearshore waves interact in space and time and how they influence the form and distribution of beaches.

An EOF analysis is used to examine the link between grain size, beach-face slope, and regional climate, focusing on how well the latter predicts the dynamics of the former two. This method is advantageous because it provides a framework for defining beach morphology as a function of climatic change and a broad overview of grain size and slope distribution on sandy beaches. During the Southwest and Northeast monsoons, the onshore push of the divergent wave is evident, showing that both seasonal climates have a role in modifying the beach-face morphology. The EOF data enabled us to understand the current condition of beach face variability with seasonal changes. According to the results of the CCA, the mean wave energy, the wave energy flux, and the beach face slope all indicate an immediate response with a significant association. However, there is an inverse link between the median particle size of sediment and dimensionless fall velocity. Although specific times of morphological change are not readily identifiable in the sedimentary signal, there are several locations where temporal variations in the sedimentology are connected to the morphological response along the beach face. This suggests a link between beach face modification, wave activity, sediment characteristics, and the beach face. The beach slopes along the coast of Goa saw a seasonal increase during the NE and SW monsoons and recuperation prior to the monsoons (PRM). The current findings will be a foundation for further in-depth research into beach modification and sediment transition under wave-dominated processes. Initial temporal EOF was highly linked with beach volume trends at each site, suggesting that this could be a valuable index for beach health.

Conflict Of Interest

The authors declare that they have no conflict of i

Funding

The authors declare that no funds, grants, or other support were received during the preparation of this manuscript.

Declaration Of Competing Interest

The authors declare that they have no known competing financial interests or personal relationships that could have appeared to influence the work reported in this paper.

Author Contributions

All authors contributed to the study's conception and design. Conceptualisation: [LEO and JKS]; Methodology: [LEO]; Formal analysis and investigation: [LEO]; Writing - original draft preparation:

[LEO]; Writing - review and editing: [JKS]; Supervision: [JKS]. All authors read and approved the final manuscript.

Data Availability

The datasets generated during and analysed during the current study are available from the corresponding author upon reasonable request.

Acknowledgments

The authors acknowledge the support and facilities provided by the CSIR-National Institute of Oceanography. **Lynda-Uta Edet Okon** acknowledges the CSIR-TWAS Fellowship. The help rendered by the staff of the Ocean Engineering Division, CSIR-NIO, is placed on record for their assistance in field and laboratory analysis. This article forms a part of the PhD thesis of the first author, registered at the Bharathidasan University, India. CSIR-NIO contribution number is _____ (will be filled after acceptance of manuscript).

nterest.

References

- Aagaard T (2014) Journal of Geophysical Research : Earth Surface. J Geophys Res Earth Surf 300–316. <https://doi.org/10.1002/2013JF002871>.Received
- Ahmed E (1972) Coastal Geomorphology of India. Orient Longman, New Delhi
- Anoop T, V SK, Shanas P, Johnson G (2015) Surface wave climatology and its variability in the North Indian Ocean based on ERA-interim reanalysis. J Atmos Ocean Technol 32:1372–1385. <https://doi.org/10.1175/JTECH-D-14-00212.1>
- Aparna M, Shetye S, Shankar D, et al (2005) Estimating The Seaward Extent Of Sea Breeze From Quikscat Scatterometry. Geophys Res Lett 32:L13601. <https://doi.org/10.1029/2005gl023107>
- Azidane H, Benmohammad A, Michel B, Bouhaddioui M El (2021) Equilibrium beach profile on sandy beach of the Mehdy coast of Morocco. 03008:9–12
- Baiyegunhi TL, Liu K, Gwavava O, Baiyegunhi C (2020) Textural characteristics, mode of transportation and depositional environment of the Cretaceous sandstone in the Bredasdorp Basin, off the south coast of South Africa: Evidence from grain size analysis. Open Geosci 12:1512-1532. <https://doi.org/https://doi.org/10.1515/geo-2020-0135>
- Bascom W (1951a) The relation between sand size and beach face slope. Trans Am Geophys Union 32:866–874
- Bascom W (1951b) The relationship between sand size and beach-face slope. 32:866–874. <https://doi.org/https://doi.org/10.1029/TR032i006p00866>

- Berg-Sørensen K, Flyvbjerg H (2005) The colour of thermal noise in classical Brownian motion: a feasibility study of direct experimental observation. *New J Phys* 7:38–38. <https://doi.org/10.1088/1367-2630/7/1/038>
- Bergillos RJ, Masselink G, Ortega-Sánchez M (2017) Coupling cross-shore and longshore sediment transport to model storm response along a mixed sand-gravel coast under varying wave directions. *Coast Eng* 129:93–104. <https://doi.org/10.1016/j.coastaleng.2017.09.009>
- Blott S, Pye K (2001a) GRADISTAT: A GRAIN SIZE DISTRIBUTION AND STATISTICS PACKAGE FOR THE ANALYSIS OF UNCONSOLIDATED SEDIMENTS. *Earth Surf Process Landforms* 26:1237–1248. <https://doi.org/10.1002/esp.261>
- Blott S, Pye K (2001b) Gradistat: A Grain Size Distribution And Statistics Package For The Analysis Of Unconsolidated Sediments. *Earth Surf Process Landf* 26:1237–12:26:1237–1248
- Bujan N, Cox R, Masselink G (2019) From fine sand to boulders: Examining the relationship between beach-face slope and sediment size. *Mar Geol* 417:106012. <https://doi.org/10.1016/j.margeo.2019.106012>
- Buscombe D, Masselink G (2006) Concepts in gravel beach dynamics. *Earth-Science Rev* 79:33–52. <https://doi.org/10.1016/j.earscirev.2006.06.003>
- Cabezas-Rabadán C, Pardo-Pascual JE, Palomar-Vázquez J (2021) Characterising the relationship between the sediment grain size and the shoreline variability defined from sentinel-2 derived shorelines. *Remote Sens* 13:. <https://doi.org/10.3390/rs13142829>
- Chatzirodou A, Karunarathna H, Reeve DE (2017) Modelling 3D hydrodynamics governing island-associated sandbanks in a proposed tidal stream energy site. *Appl Ocean Res* 66:79–94. <https://doi.org/10.1016/j.apor.2017.04.008>
- Chempalayil SP, Kumar VS, Dora GU, Johnson G (2014) Near shore waves, long-shore currents and sediment transport along micro-tidal beaches, central west coast of India. *Int J Sediment Res* 29:402–413. [https://doi.org/10.1016/S1001-6279\(14\)60054-8](https://doi.org/10.1016/S1001-6279(14)60054-8)
- Cheng HQ, Chen W, Li JF, et al (2022) Morphodynamic changes in the Yangtze Estuary under the impact of the Three Gorges Dam, estuarine engineering interventions and climate-induced sea level rise. *Earth Planet Sci Lett* 580:. <https://doi.org/10.1016/j.epsl.2022.117385>
- Chowdhury P, Behera MR, Reeve DE (2020) Future wave-climate driven longshore sediment transport along the Indian coast. *Clim Change* 162:405–424. <https://doi.org/10.1007/s10584-020-02693-7>
- Cohen O (2015) Profiler 3.1 XL, a free software for the construction and analysis of profiles Civil, maps in Microsoft Excel. *Acts XIIIeNational Coast Eng Days – Eng Dunkirk*
- Conlin MP, Adams PN, Jaeger JM, MacKenzie R (2020) Quantifying Seasonal-to-Interannual-Scale Storm Impacts on Morphology Along a Cuspate Coast With a Hybrid Empirical Orthogonal Function Approach. *J Geophys Res Earth Surf* 125:. <https://doi.org/10.1029/2020JF005617>
- Dean RG, Dalrymple RA (2010) Equilibrium Beach Profiles. *Coast Process with Eng Appl* 162–209. <https://doi.org/10.1017/cbo9780511754500.008>

- Duane DB (1964) Significance of skewness in recent sediments, western Pamlico Sound, North Carolina. *J Sediment Pet* 34:864–74
- Dwarakish GS, Vinay SA, Natesan U, et al (2009) Coastal vulnerability assessment of the future sea level rise in Udupi coastal zone of Karnataka state, west coast of India. *Ocean Coast Manag* 52:467–478. <https://doi.org/10.1016/j.ocecoaman.2009.07.007>
- Elias EPL, Hansen JE (2013) Understanding processes controlling sediment transports at the mouth of a highly energetic inlet system (San Francisco Bay, CA). *Mar Geol* 345:207–220. <https://doi.org/10.1016/j.margeo.2012.07.003>
- Fernandes LL, Rao VP, Kessarkar PM, Suresh S (2018) Estuarine turbidity maximum in six tropical minor rivers, central west coast of India. *Hydrol Res* 49:1234–1254. <https://doi.org/10.2166/nh.2017.031>
- Folk R, Ward W (1957a) Brazos River Bar : A Study in the Significance of Grain-Size Parameters. *J Sediment Petrol* 27:3–26
- Folk RL and, Ward WC (1957b) B R A Z O S R I V E R B A R : A S T U D Y I N T H E S I G N I F I C A N C E O F G R A I N S I Z E P A R A M E T E R S C . W A R D bar also afforded an opportunity to study the reason for the peculiar , almost universal lack of s e d i m e n t a r y particles in th. *J Sediment Petrol* 27:3–26
- Fredriksson C, Larson M, Hanson H (2017) Long-Term Modelling of Aeolian Transport and Beach-Dune Evolution. *Coast Dyn* 715–726
- Friedman GM, Sanders JE (1978) *Principles of Sedimentology*. Wiley, New York.
- Gao S, Collins MB (1994) Analysis of Grain Size Trends, for Defining Sediment Transport Pathways in Marine Environments. *J Coast Res* 10:70–78.
- Gerald M. Friedman (1967) Dynamic Processes and Statistical Parameters Compared for Size Frequency Distribution of Beach and River Sands. *SEPM J Sediment Res Vol. 37*: <https://doi.org/10.1306/74d716cc-2b21-11d7-8648000102c1865d>
- Glejin J, Sanil Kumar V, Balakrishnan Nair TM, Singh J (2013) Influence of winds on temporally varying short and long period gravity waves in the near shore regions of the eastern Arabian Sea. *Ocean Sci* 9:343–353. <https://doi.org/10.5194/os-9-343-2013>
- GOURLAY MR (1968) Beach and Dune Erosion Tests.
- Hallin C, Almström B, Larson M, Hanson H (2019) Longshore transport variability of beach face grain size: Implications for dune evolution. *J Coast Res* 35:751–764. <https://doi.org/10.2112/JCOASTRES-D-18-00153.1>
- Harley MD, Turner IL, Short AD, Ranasinghe R (2011) Assessment and integration of conventional, RTK-GPS and image-derived beach survey methods for daily to decadal coastal monitoring. *Coast Eng* 58:194–205
- Hegde VS, Nayak SR, Huchchannavar GK, et al (2022) Meso-scale foreshore evolution in low-energy, storm-dominated tropical west coast of India: Implications for shoreline management. *J Earth Syst Sci* 131:. <https://doi.org/10.1007/s12040-021-01773-1>

- Hein CJ, Fallon AR, Rosen P, et al (2019) Shoreline dynamics along a developed river mouth barrier island: Multi-decadal cycles of erosion and event-driven mitigation. *Front Earth Sci* 7:1–23. <https://doi.org/10.3389/feart.2019.00103>
- Jayakumar S, Raju N, Gowthaman R, et al (2001) Daily beach profiles and littoral environmental observations off Baga, Calangute and Miramar beaches during February–March 1999. Dona Paula, Goa (India)
- Joevivek V, Chandrasekar N, Saravanan S, et al (2018) Spatial and temporal correlation between beach and wave processes: implications for bar–berm sediment transition. *Front Earth Sci* 12:349–360. <https://doi.org/10.1007/s11707-017-0655-y>
- Joevivek VJ, Chandrasekar N, Jayangondaperumal R, et al (2019) An interpretation of wave refraction and its influence on foreshore sediment distribution. *Acta Oceanol Sin* 38:151–160. <https://doi.org/10.1007/s13131-019-1446-y>
- Karunaratna H, Horrillo-Caraballo J, Kuriyama Y, et al (2016) Linkages between sediment composition, wave climate and beach profile variability at multiple timescales. *Mar Geol* 381:194–208. <https://doi.org/10.1016/j.margeo.2016.09.012>
- Karunaratna H, Horrillo-Caraballo JM, Ranasinghe R, et al (2012a) An analysis of the cross-shore beach morphodynamics of a sandy and a composite gravel beach. *Mar Geol* 299–302:33–42. <https://doi.org/10.1016/j.margeo.2011.12.011>
- Karunaratna H, Horrillo-Caraballo JM, Ranasinghe R, et al (2012b) An analysis of the cross-shore beach morphodynamics of a sandy and a composite gravel beach. *Mar Geol* 299–302:33–42. <https://doi.org/10.1016/j.margeo.2011.12.011>
- Karunaratna H, Kuriyama Y, Mase H, et al (2015a) Forecasts of seasonal to inter-annual beach change using a reduced physics beach profile model. *Mar Geol* 365:14–20. <https://doi.org/10.1016/j.margeo.2015.03.009>
- Karunaratna H, Ranasinghe R, Reeve DE (2015b) A hybrid beach morphology model applied to a high energy sandy beach. *Ocean Dyn* 65:1411–1422. <https://doi.org/10.1007/s10236-015-0884-0>
- Karunaratna H, Reeve DE (2013) A hybrid approach to model shoreline change at multiple timescales. *Cont Shelf Res* 66:29–35. <https://doi.org/10.1016/j.csr.2013.06.019>
- Karunaratna HU, Mase H, Baba Y (2015c) Analysis of multi-scale morphodynamic behavior of a high energy beach facing the Sea of Japan. *Front Mar Sci* 2:1–10. <https://doi.org/10.3389/fmars.2015.00051>
- Komar PD, Gaughan MK. (1972) AIRY WAVE THEORY AND BREAKER HEIGHT PREDICTION. *Environ Sci*
- Krumbein W C (1934) Size frequency distributions of sediments. *J Sediment Petrol* 4:65–77
- Kunte PD, Jauhari N, Mehrotra U, et al (2014a) Multi-hazards coastal vulnerability assessment of Goa, India, using geospatial techniques. *Ocean Coast Manag* 95:264–281. <https://doi.org/10.1016/j.ocecoaman.2014.04.024>

- Kunte PD, Jauhari N, Mehrotra U, et al (2014b) Multi-hazards coastal vulnerability assessment of Goa, India, using geospatial techniques. *Ocean Coast Manag* 95:264–281. <https://doi.org/10.1016/J.OCECOAMAN.2014.04.024>
- Larson M, Bayram A (2005) Calculating Cross-shore Distribution of Longshore Sediment Transport. *J Coast Res* 203
- Larson M, C. Kraus N (1995) Prediction of cross-shore sediment transport at different spatial and temporal scales. *Mar Geol* 126:111–127. [https://doi.org/10.1016/0025-3227\(95\)00068-A](https://doi.org/10.1016/0025-3227(95)00068-A)
- Larson M, Capobianco M, Hanson H (2000) Relationship between beach profiles and waves at Duck, North Carolina, determined by canonical correlation analysis. *Mar Geol* 163:275–288. [https://doi.org/10.1016/S0025-3227\(99\)00119-X](https://doi.org/10.1016/S0025-3227(99)00119-X)
- Larson M, Capobianco M, Jansen H, et al (2003) Analysis and Modeling of Field Data on Coastal Morphological Evolution over Yearly and Decadal Time Scales. Part 1: Background and Linear Techniques. *J Coast Res* 19:760–775
- Lemke L, Miller JK, Mahon A, Livermont E (2014) Eof Analysis of Shoreline Changes Following an Alternative Beach Fill Within a Groin Field. *Coast Eng Proc* 1:83. <https://doi.org/10.9753/icce.v34.sediment.83>
- Lemos C, Floch F, Yates M, et al (2018) Equilibrium modeling of the beach profile on a macrotidal embayed low tide terrace beach. *Ocean Dyn* 68:1207–1220. <https://doi.org/10.1007/s10236-018-1185-1>
- Ludka BC, Guza RT, O'Reilly WC, Yates ML (2015) *Journal of Geophysical Research : Oceans*. *J Geophys Res Ocean* 2813–2825. <https://doi.org/10.1002/2015JC010893>.Received
- Luijendijk A, Hagenaars G, Ranasinghe R, et al (2018) The State of the World's Beaches. *Sci Rep* 8:1–11. <https://doi.org/10.1038/s41598-018-24630-6>
- Mahmood AB, Abdullah SS (2016) Breaker wind waves energy at Iraqi coastline
- Mangor K, Drønen NK, Kærgaard KH, Kristensen SE (2017) Shoreline management guidelines
- Martínez ML, Psuty NP, Lubke RA (2008) A Perspective on Coastal Dunes. 3–10. https://doi.org/10.1007/978-3-540-74002-5_1
- Mascarenhas A (1999) The Coastal Regulation Zone of Goa: Oceanographic, environmental and societal perspectives. *Curr Sci* 77:1598–1605
- MASCARENHAS A (1998) Study of Goa and its Environment from Space. *Natl Inst Oceanogr*
- Masselink G, Austin M, Tinker J, et al (2008) Cross-shore sediment transport and morphological response on a macrotidal beach with intertidal bar morphology, Truc Vert, France. *Mar Geol* 251:141–155. <https://doi.org/10.1016/j.margeo.2008.01.010>
- McCall RT, Masselink G, Poate TG, et al (2015) Modelling the morphodynamics of gravel beaches during storms with XBeach-G. *Coast Eng* 103:52–66. <https://doi.org/10.1016/j.coastaleng.2015.06.002>

- McFall BC (2019) The Relationship between Beach Grain Size and Intertidal Beach Face Slope. *J Coast Res* 35:1080–1086. <https://doi.org/10.2112/JCOASTRES-D-19-00004.1>
- Medellín G, Torres-Freyermuth A (2019) Morphodynamics along a micro-tidal sea breeze dominated beach in the vicinity of coastal structures. *Mar Geol* 417:106013. <https://doi.org/10.1016/j.margeo.2019.106013>
- Medellín G, Torres-Freyermuth A, Tomasicchio GR, et al (2018) Field and numerical study of resistance and resilience on a sea breeze dominated beach in Yucatan (Mexico). *Water (Switzerland)* 10:. <https://doi.org/10.3390/w10121806>
- Miles A, Ilic S, Whyatt D, James MR (2019) Characterising beach intertidal bar systems using multi-annual LiDAR data. *Earth Surf Process Landforms* 44:1572–1583. <https://doi.org/10.1002/esp.4594>
- Miller JK, Dean RG (2007) Shoreline variability via empirical orthogonal function analysis: Part I temporal and spatial characteristics. *Coast Eng* 54:111–131. <https://doi.org/10.1016/j.coastaleng.2006.08.013>
- MILLER JK, LEMKE L, LAPANN-JOHANNESSEN C, LIVERMONT E (2015) Application of Eof Analysis To the Evolution of a Feeder Beach Constructed Within a Groin Field. 1–13. https://doi.org/10.1142/9789814689977_0033
- Muñoz-Perez JJ, Medina R (2010) Comparison of long-, medium- and short-term variations of beach profiles with and without submerged geological control. *Coast Eng* 57:241–251. <https://doi.org/10.1016/j.coastaleng.2009.09.011>
- Nadaf FM (2019) Geographical Analysis of the Coastal Landforms of Canacona, Goa. *Int J Multidiscip* 4:655–661
- Niraj PS, Balaji R, Vethamony P (2015) Pre-monsoon hydrodynamic modeling of Goa coast, West coast of India. *ISH J Hydraul Eng* 21:276–286. <https://doi.org/10.1080/09715010.2015.1017747>
- North GR, Bell TL, Cahalan RF (1982) Sampling errors in the estimation of empirical orthogonal functions. *Am Meteorol Soc Mon Weather Rev* 110:699–706
- Noujas V, Kankara RS, Rasheed K (2018) Estimation of Longshore Sediment Transport Rate for a Typical Pocket Beach Along West Coast of India. *Mar Geod* 41:201–216. <https://doi.org/10.1080/01490419.2017.1422818>
- Okon L-UE, Seelam JK, Kumari S, Hemanath L (2023) Sediment dynamics of tropical open coast beaches , central west coast of India : implications of spatio - temporal variability. *Geo-Marine Lett* 1–17. <https://doi.org/10.1007/s00367-023-00746-1>
- Oliveira S, Moura D, Horta J, et al (2017) The morphosedimentary behaviour of a headland–beach system: Quantifying sediment transport using fluorescent tracers. *Mar Geol* 388:62–73. <https://doi.org/10.1016/j.margeo.2017.02.010>
- Reeve DE, Karunarathna H, Pan S, et al (2016) Data-driven and hybrid coastal morphological prediction methods for mesoscale forecasting. *Geomorphology* 256:49–67. <https://doi.org/10.1016/j.geomorph.2015.10.016>

- Reis AH, Gama C (2010) Sand size versus beachface slope - An explanation based on the Constructal Law. *Geomorphology* 114:276–283. <https://doi.org/10.1016/j.geomorph.2009.07.008>
- Sanil Kumar V, Pathak KC, Pednekar P, et al (2006) Coastal processes along the Indian coastline. *Curr Sci* 91:530–536
- Seelam JK, Yadhunath EM, Jishad M, et al (2014) Post-monsoon equilibrium beach profiles and longshore sediment transport rates at Candolim, Miramar and Keri beaches of Goa, India. *Curr Sci* 106:408–416. <https://doi.org/10.18520/cs/v106/i3/408-416>
- Senechal N, Ruiz de Alegría-Arzaburu A (2020) Seasonal imprint on beach morphodynamics. Elsevier Ltd
- Shanas PR, Sanil Kumar V (2014) Coastal processes and longshore sediment transport along Kundapura coast, central west coast of India. *Geomorphology* 214:436–451. <https://doi.org/10.1016/J.GEOMORPH.2014.02.027>
- Short AD (1993) Beach and Surf Zone Morphodynamics. *J Coast Res* 15:25–37
- Stive MJF, de Vriend HJ (1995) Modelling shoreface profile evolution. *Mar Geol* 126:235–248. [https://doi.org/10.1016/0025-3227\(95\)00080-I](https://doi.org/10.1016/0025-3227(95)00080-I)
- Tamura T, Nicholas WA, Oliver TSN, Brooke BP (2018) Coarse-sand beach ridges at Cowley Beach, north-eastern Australia: Their formative processes and potential as records of tropical cyclone history. *Sedimentology* 65:721–744. <https://doi.org/10.1111/sed.12402>
- Tucker M (1990) Techniques in sedimentology.
- Veerayya M, Murty CS, Varadachari VVR (1981) Sediment dis-tribution in the offshore regions of Goa. *Indian J Mar Sci* 10:332-336.
- Vos K, Harley MD, Splinter KD, et al (2020) Beach Slopes From Satellite-Derived Shorelines. *Geophys Res Lett* 47:. <https://doi.org/10.1029/2020GL088365>
- Wagle B (1993) Geomorphology of Goa and Goa Coast: A Review. *Mus Geol Di Bol*
- Wilson JSJ, Sujitha SB, Shruti VC, et al (2014) Seasonal variability of beach characteristics between Candoliam and Colva coast, Goa, India. *J Coast Sci* 1:33–40
- Winant CD, Inman DL, Nordstrom CE (1975) Description of Seasonal Beach Changes Using Empirical Eigenfunction. *J Geophys Res* 80:1979–1986
- Woodruff JD, Venti NL, Mabee SB, et al (2021a) Grain size and beach face slope on paraglacial beaches of New England, USA. *Mar Geol* 438:106527. <https://doi.org/10.1016/j.margeo.2021.106527>
- Woodruff JD, Venti NL, Mabee SB, et al (2021b) Grain size and beach face slope on paraglacial beaches of New England, USA. *Mar Geol* 438:106527. <https://doi.org/10.1016/j.margeo.2021.106527>

Wright LD, Short AD (1984) Morphodynamic variability of surf zones and beaches: A synthesis. *Mar Geol* 56:93–118. [https://doi.org/10.1016/0025-3227\(84\)90008-2](https://doi.org/10.1016/0025-3227(84)90008-2)

Yadhunath EM, Seelam JK, M. J (2022) Rip current occurrences in meso tidal surf zones at a coastal stretch along the central west coast of India. *Reg Stud Mar Sci* 51:102180. <https://doi.org/10.1016/j.rsma.2022.102180>

Figure A1 —Beach profiles of selected beaches in North and South Goa

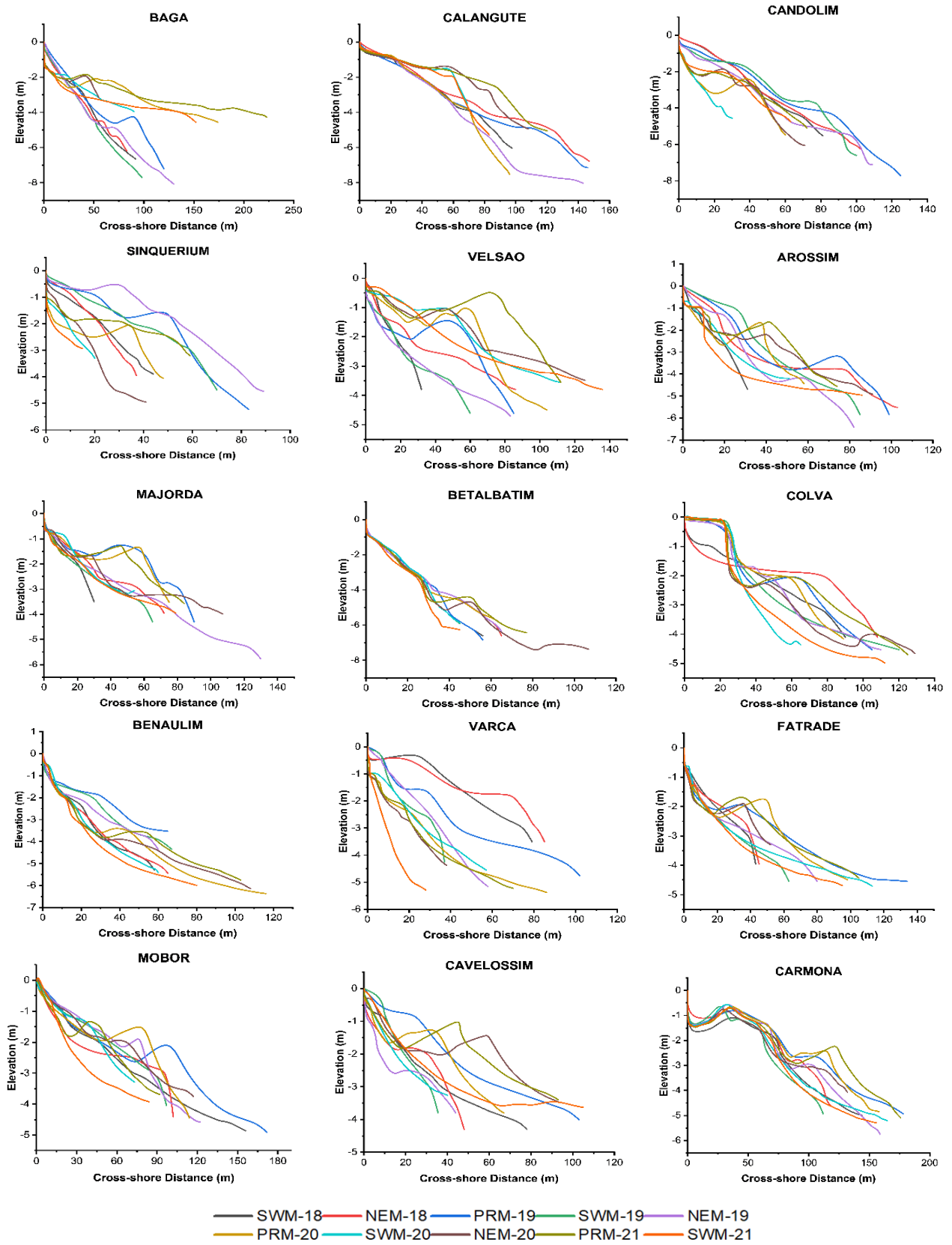


Table A1 — Summary statistics for sedimentologic parameters for North and South Goa beaches

SWM		D ₁₀	D ₅₀	D ₉₀	D ₉₀ /D ₁₀	D ₈₄ /D ₁₆	Sorting		Skewness		Kurtosis	
North Goa	BAG	0.37	0.25	0.16	0.46	0.55	0.46	WS	0.06	SYM	1.09	MSK
	CAL	0.37	0.31	0.16	0.46	0.55	0.46	WS	0.00	SYM	1.17	LPK
	CAN	0.61	0.39	0.26	0.45	0.55	0.45	WS	0.01	SYM	1.12	LPK
	SINQ	0.72	0.42	0.25	0.39	0.50	0.54	MWS	-0.12	CSK	1.41	LPK
South Goa	VEL	0.42	0.35	0.16	0.41	0.50	0.51	MWS	-0.06	SYM	1.03	MSK
	ARO	0.38	0.34	0.16	0.38	0.48	0.56	MWS	-0.18	CSK	1.13	LPK
	MAJ	0.29	0.19	0.14	0.46	0.61	0.45	WS	-0.12	CSK	1.47	LPK
	BET	0.29	0.20	0.14	0.43	0.54	0.48	WS	-0.05	SYM	1.16	LPK
	COL	0.31	0.19	0.14	0.52	0.61	0.39	WS	-0.02	SYM	1.19	LPK
	BEN	0.68	0.28	0.16	0.35	0.44	0.65	MWS	-0.09	SYM	1.01	MSK
	VAR	0.27	0.25	0.14	0.47	0.60	0.42	WS	0.22	VFSK	1.58	VLP
	FATR	0.28	0.19	0.13	0.42	0.54	0.57	MWS	-0.19	CSK	1.61	VLP
	CAR	0.25	0.18	0.13	0.52	0.61	0.41	WS	0.03	SYM	1.24	LPK
	CAV	0.30	0.22	0.15	0.50	0.59	0.39	WS	0.06	SYM	1.00	MSK
	MOB	0.30	0.20	0.15	0.55	0.63	0.34	VWS	0.05	SYM	1.08	MSK
NEM												
North Goa	BAG	0.58	0.22	0.17	0.31	0.31	1.00	MS	-0.66	VCSK	1.37	LPK
	CAL	0.39	0.23	0.17	0.29	0.40	0.70	MWS	-0.58	VCSK	1.18	LPK
	CAN	0.81	0.39	0.22	0.55	0.66	1.03	MS	-0.21	CSK	1.20	LPK
	SINQ	0.51	0.22	0.17	0.74	0.77	0.63	MWS	0.17	CSK	0.83	PLK
South Goa	VEL	0.52	0.21	0.18	0.36	0.36	1.00	MS	-0.61	VCSK	1.31	LPK
	ARO	0.32	0.22	0.14	0.49	0.65	0.40	VWS	-0.34	VCSK	1.56	VLP
	MAJ	0.41	0.22	0.15	0.57	0.71	0.46	VWS	-0.15	CSK	1.50	VLP
	BET	0.35	0.26	0.25	0.34	0.48	0.67	MWS	-0.20	CSK	1.62	VLP
	COL	0.55	0.28	0.16	0.14	0.31	1.03	MS	-0.73	VCSK	1.58	VLP
	BEN	0.60	0.24	0.17	0.29	0.37	1.59	MS	-1.15	CSK	1.47	LPK
	VAR	0.53	0.27	0.21	0.12	0.22	1.13	MS	-0.47	VCSK	1.31	LPK
	FATR	0.31	0.23	0.17	0.33	0.43	0.61	MWS	-0.08	SYM	1.04	MSK
	CAR	0.34	0.21	0.13	0.40	0.53	0.53	MWS	-0.17	CSK	1.47	LPK
	CAV	0.45	0.28	0.17	0.40	0.49	0.53	MWS	-0.08	SYM	1.08	MSK
	MOB	0.42	0.32	0.16	0.54	0.62	0.32	VWS	-0.16	CSK	0.97	MSK
PRM												
North Goa	BAG	0.48	0.24	0.17	0.43	0.52	0.75	MWS	-0.15	CSK	1.09	MSK
	CAL	0.47	0.25	0.19	0.43	0.38	0.79	MWS	0.10	SYM	1.19	LPK
	CAN	0.52	0.25	0.19	0.48	0.48	0.54	MWS	-0.21	CSK	1.06	MSK
	SINQ	0.56	0.27	0.18	0.29	0.36	0.82	MWS	-0.54	VCSK	0.65	VPLK
South Goa	VEL	0.58	0.23	0.14	0.33	0.43	0.65	MWS	-0.23	CSK	1.27	LPK
	ARO	0.52	0.21	0.16	0.36	0.39	1.07	MS	-0.69	VCSK	1.73	VLP
	MAJ	0.48	0.21	0.13	0.54	0.67	0.35	WS	-0.01	SYM	1.38	LPK

	BET	0.30	0.19	0.13	0.60	0.67	0.29	VWS	0.03	SYM	1.02	MSK
	COL	0.43	0.20	0.14	0.40	0.32	1.07	MS	-0.68	VCSK	2.45	VLP
	BEN	0.33	0.22	0.13	0.44	0.54	0.51	MWS	-0.64	VCSK	1.35	LPK
	VAR	0.53	0.24	0.16	0.49	0.60	0.40	WS	-0.30	CSK	1.33	LPK
	FATR	0.44	0.19	0.15	0.49	0.59	0.40	WS	-0.06	SYM	1.10	MSK
	CAR	0.44	0.20	0.14	0.56	0.64	0.33	WS	-0.02	SYM	1.04	MSK
	CAV	0.27	0.19	0.13	0.51	0.60	0.38	WS	-0.08	SYM	1.08	MSK
	MOB	0.28	0.21	0.13	0.55	0.64	0.36	WS	-0.10	SYM	1.20	LPK

**Ws-well sorted; vws-very well sorted; ms-doderately sorted; mws-moderately well sorted; sym-symmetric; csk- coarse skewed; vcsk-very coarse skewed; vlp-very leptokurtic; msk-mesokurtic;lpk-leptokurtic; plk-platykurtic; vlp-very platikurtc*